AD-A171 734 EFFECTS OF SMALL NOSE BLUNTNESS ON STATIC STABILITY AND MAGNUS CHARACTERI.. (U) ARMY BALLISTIC RESEARCH LAB ABERDEEN PROVING GROUND MD L D KAYSER JUL 86 1/1

UNCLASSIFIED BRL-MR-3535 F/G 19/1 NL

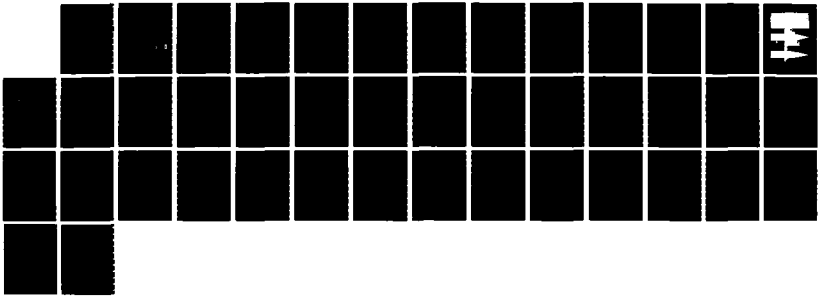

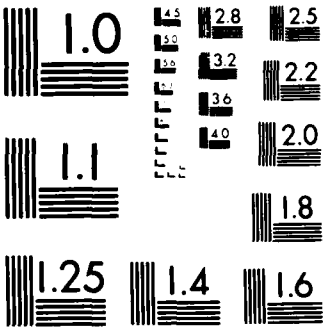

(12)

US ARMY
MATERIEL
COMMAND

AD

MEMORANDUM REPORT BRL-MR-3535

AD-A171 734

EFFECTS OF SMALL NOSE BLUNTNESS ON STATIC STABILITY AND MAGNUS CHARACTERISTICS OF A PROJECTILE SHAPE AT MACH 0.91 AND 3.03

Lyle D. Kayser

July 1986

US ARMY BALLISTIC RESEARCH LABORATORY
ABERDEEN PROVING GROUND, MARYLAND

UNCLASSIFIED
SECURITY CLASSIFICATION OF THIS PAGE

AD-A171734

REPORT DOCUMENTATION PAGE

Form Approved
OMB No 0704-0188
Exp. Date Jun 30, 1986

1a. REPORT SECURITY CLASSIFICATION UNCLASSIFIED	1b. RESTRICTIVE MARKINGS
2a. SECURITY CLASSIFICATION AUTHORITY	3. DISTRIBUTION/AVAILABILITY OF REPORT Approved for public release, distribution unlimited.
2b. DECLASSIFICATION/DOWNGRADING SCHEDULE	
4. PERFORMING ORGANIZATION REPORT NUMBER(S) Memorandum Report BRL-MR-3535	5. MONITORING ORGANIZATION REPORT NUMBER(S)
6a. NAME OF PERFORMING ORGANIZATION U.S. Army Ballistic Research Laboratory 6b. OFFICE SYMBOL (If applicable) SLCBR-LF	7a. NAME OF MONITORING ORGANIZATION
6c. ADDRESS (City, State, and ZIP Code) Aberdeen Proving Ground, Maryland 21005-5066	7b. ADDRESS (City, State, and ZIP Code)
8a. NAME OF FUNDING/SPONSORING ORGANIZATION 8b. OFFICE SYMBOL (If applicable)	9. PROCUREMENT INSTRUMENT IDENTIFICATION NUMBER
8c. ADDRESS (City, State, and ZIP Code)	10. SOURCE OF FUNDING NUMBERS PROGRAM ELEMENT NO. 62618A; PROJECT NO. 1L162618AH80; TASK NO. 00; WORK UNIT ACCESSION NO 001 A1

11. TITLE (Include Security Classification)
EFFECTS OF SMALL NOSE BLUNTNESS ON STATIC STABILITY AND MAGNUS CHARACTERISTICS OF A PROJECTILE SHAPE AT MACH 0.91 AND 3.03

12. PERSONAL AUTHOR(S)
KAYSER, LYLE D.

13a. TYPE OF REPORT	13b. TIME COVERED	14. DATE OF REPORT (Year, Month, Day)	15. PAGE COUNT
Memorandum Report	FROM _____ TO _____	July 1986	41

16. SUPPLEMENTARY NOTATION

17. COSATI CODES			18. SUBJECT TERMS (Continue on reverse if necessary and identify by block number)
FIELD	GROUP	SUB-GROUP	
01	01		Aerodynamic Forces; Magnus Force
20	04		Spinning Projectile; Wind Tunnel Test
			Supersonic; Transonic

19. ABSTRACT (Continue on reverse if necessary and identify by block number)

Wind tunnel test results on a typical projectile shape with small nose bluntness are reported. Flat and hemispherical nose tip results are shown in addition to sharp nose tip results. The effects of nose bluntness on static stability are shown to be negligible at both Mach 0.91 and 3.02 . The effects of nose bluntness on Magnus force and Magnus moment were not large, but of sufficient magnitude to indicate that such bluntness should not be neglected in a numerical flow field computation.

20. DISTRIBUTION/AVAILABILITY OF ABSTRACT	21. ABSTRACT SECURITY CLASSIFICATION
☒ UNCLASSIFIED/UNLIMITED ☐ SAME AS RPT ☐ DTIC USERS	UNCLASSIFIED
22a. NAME OF RESPONSIBLE INDIVIDUAL LYLE D. KAYSER	22b TELEPHONE (Include Area Code) (301) 278-3815 22c OFFICE SYMBOL SLCBR-LF

DD FORM 1473, 84 MAR

83 APR edition may be used until exhausted
All other editions are obsolete

SECURITY CLASSIFICATION OF THIS PAGE
UNCLASSIFIED

SUMMARY

1. For purposes of computational modeling, the effects of nose bluntness cannot be ignored.

2. The effect of blunting the nose tip is to increase the Magnus force. No large or consistent effect of nose tip bluntness on yawing moment or side force center of pressure was observed.

3. The effect of nose tip bluntness on pitch plane force and moment data was found to be small.

4. The results of the present investigation are consistent with findings of Dolling's nose tip bluntness investigation.

5. The side force center of pressure data at small pd/V and small α are not considered reliable.

TABLE OF CONTENTS

LIST OF ILLUSTRATIONS

LIST OF ILLUSTRATIONS (Continued)

LIST OF TABLES

I. INTRODUCTION

A theoretical and experimental research program has been underway in the Launch and Flight Division of US Army Ballistic Research Laboratory (BRL), Aberdeen Proving Ground, MD, in recent years to provide the capability of predicting projectile aerodynamics. The direction of the predictive capability is generally toward the use of modern finite-difference computational techniques. The primary objective of the experimental program is to obtain data for comparison with computations. The ogive-cylinder-boattail shape of Figure 1 was chosen because a substantial amount of experimental and computational data already exist for this shape which is typical of modern low drag shell.

The three nose tip configurations are shown in Figure 2; the flat nose tip is typical of a projectile fuze meplat. Parabolized Navier Stokes computations are being used for supersonic flow field computations and time-dependent Navier Stokes Computations are being used for transonic flowfields, including base flows. These computations can often be facilitated by the use of a sharp nose tip approximation or by a spherical nose tip approximation but only if no significant error is introduced.

II. EXPERIMENT

1. MODELS AND INSTRUMENTATION

The geometry of the ogive-cylinder-boattail configuration (SOCBT) is shown in Figure 1. The ogive-cylinder (SOC) is identical except that the boattail is zero degrees. The Model was equipped with a boundary layer trip which was located 1.15 caliber from the tip of the sharp nosed configuration for the M = 3.02 test runs. The boundary layer trip was not used for the the transonic test runs. Three nose tips were tested as seen in the shadow-graph of Figure 2. The height of the flat and spherical portions of the nose tip was 0.1 caliber at the intersection of the ogive. The model was equipped with an air turbine system for spinning the model to approximately 700 rps as required for the Magnus test runs. An internal strain-gage balance capable of measuring normal force, pitching moment, side force, and yawing moment was supplied by the Naval Surface Weapons Center (NSWC), Silver Spring, MD.

2. WIND TUNNELS

The tests were conducted in the NSWC Tunnel No. 2 which is a 0.41 x 0.41m (16 x 16 inch) cross section, horizontal tunnel with an open jet test section capable of operation over a Mach number range of 0.3 to 5.02 with supply pressures ranging from 0.5 to 15 atmospheres. The tunnel is capable of intermittent (blowdown) or continuous operation with a higher Reynolds capability for the intermittent mode. Mach number changes are made by replacing the two-dimensional nozzle block units -- each nozzle block provides one distinct Mach number.

3. PROCEDURES

Supply pressure for the Mach 0.91 test runs was set at one atmosphere and the supply temperature was typically 300 k (80 deg F). For the Mach 3.02 test runs, supply pressure was set at 138×10^3 kPa (20 psia) and the supply temperature was typically 306 k (90 deg F). These conditions provided Reynolds numbers of 4.5×10^6 at Mach 0.91 and 2.2×10^6 at Mach 3.02 based on the model length. Data for the static stability phase of the program was acquired by pitching the model from -5 to +15 degrees and recording data continuously at the rate of 10 samples per second -- this procedure provided approximately 80 points for each pitch run. Data for the Magnus phase of the test programs were acquired by setting the model at a given angle of attack, applying turbine air to bring the model up to the desired spin rate, cutting off the turbine air supply and allowing the spin rate to decay to zero. Data were recorded during the spin down at the rate of 10 samples per second which typically yielded 350 samples at Mach 0.91 and 700 samples at Mach 3.02.

The static stability data, as a function of angle of attack, and the Magnus data, as a function of pd/V, data were fitted with 5th order polynomial curves to facilitate handling and interpretation of the data. The 5th order curve fit was usually more than adequate to describe the data variations. Figure 3 is a typical set of side force data for M = 0.91 and illustrates the random noise level of the data; also, it is seen that the data do not pass through the origin. The zero term of the polynomial curve fit was discarded in order to force the data through the origin as dictated by theory. Discrete values of C_Y and C_n were obtained from the curve fitted data at a pd/V = 0.5 for Mach 0.91 and pd/V = 0.2 for Mach 3.02. The discrete values were then divided by the respective values of pd/V to obtain the coefficients of C_{Y_p} and C_{n_p}. For plots of C_{Y_p} and C_{n_p}, data were not forced through the origin.

NOTE: Curve fitted data for moment coefficients are for a cg location 3.5 cal. from the nose tip (2.5 cal. from the base). Plotted moment coefficient data are for a cg location 3.6 cal. from the nose tip (2.4 cal. from the base)

III. RESULTS

A complete set of Magnus data is given in tables 1 through 4 in the form of polynomial coefficients:

$$C_Y = a1*(pd/V) + a2*(pd/V)**2 + a3*(pd/V)**3 + \text{- - - -}$$

$$C_n = b1*(pd/V) + b2*(pd/V)**2 + b3*(pd/V)**3 + \text{- - - -}$$

Figures 4-7 show the effects of nose bluntness on normal force and center of pressure. For the SOC shape at M = 0.91, normal force is not affected and the center pressure variation is less than 0.1 caliber. For the SOCBT at M = 0.91, normal force is not affected but the center of pressure behavior between -5 and +5 degrees seems questionable. The variation of approximately 0.2

calibers in Xcp may be reasonable but the asymmetry about $\alpha = 0°$ is not expected. The asymmetry is consistent for all three nose tips which suggests a correct measurement. The asymmetry may be a hysteresis effect caused by tunnel wall interference. At M = 3.02, there are no measurable effects of nose bluntness on normal force or center of pressure for either shape. The centers of pressure are seen to be symmetric about $\alpha = 0°$ for M = 3.02.

Figures 8-9 show the effect of angle of attack on side force efficients for the sharp nose tip. For M = 0.91, the variation with angle of attack shows a consistent behavior and the effect of the boattail is seen to increase the magnitude of the side force. At M = 3.02, the magnitude of the side force is slightly smaller on the boattailed configuration. It is also noticed at M = 3.02, Figure 9, that a positive side force exists at zero degree angle of attack which suggests a phenomenon such as a flow angularity in the wind tunnel. The incremental increases in side force with increasing angle are consistent which indicates that the data are biased by an amount equal to the side force values at zero degrees.

Figures 10-11 show the effects of nose bluntness on the side force coefficient at three degrees angle of attack. The effect of bluntness is generally seen to increase the magnitude of side force on both configurations both Mach numbers with the flat nose tip providing the largest effect. Yawing moment coefficient data are shown in Figures 12-13. The yawing moment coefficients on the SOC at M = 0.91 show the unusual non-linear behavior of initially decreasing with pd/V and then increasing at the higher values of pd/V. At all other conditions, the yawing moment increases nearly linearly with pd/V but there does not seem to be a consistent effect of nose bluntness. The side (Magnus) force centers of pressure are shown in Figures 14-15. Data at small pd/V do not appear too reliable but the effect of bluntness is generally to move the center of pressure forward. The effect of the boattail is to move the Magnus center of pressure aft at both Mach numbers.

Figures 16-21 provide a concise summary of all the Magnus data. Figures 16-17 show a definite influence of nose bluntness on Magnus force coefficient with the bluntness increasing the magnitude of the coefficients. Figure 17 (SOCBT) shows the non zero Magnus force coefficient at zero degree alpha and also the general bias of the data as mentioned above in conjunction with Figure 9. Magnus moment coefficients are shown in Figures 18-19 and do not show a definite trend with respect to nose bluntness. Magnus centers of pressure are shown in Figures 20-21 and are seen to be erratic at small angles of attack. The erratic behavior is a result of the bias mentioned above. The centers of pressure appear to be reliable for angles of attack greater than two degrees and do not change significantly with angle of attack. At the smaller angles of attack, the effect of bluntness is to move the center of pressure forward. As mentioned above, the effect of the boattail is to move the center of pressure aft.

Effects of nose bluntness on surface pressures and boundary layer parameters at Mach 3.0 were recently reported by Dolling, et al.[1] The results were for non-spinning axisymmetric shapes, characteristic of projectiles. Dolling concluded that "the distance for completion of enthropy wake effects on surface pressure distributions is small. Even with significant tip blunting ...". Also concluded was that "...tip bluntness has a strong influence on the development of all boundary-layer properties." If the surface pressures

are not significantly affected by nose tip bluntness, normal force and pitching moments should not be greatly affected. Results of the present investigation showed that normal force, pitching moment, and center of pressure were not affected by the two types of bluntness tested. Since the Magnus effect is a function of the boundary layer characteristics, it could be expected, according to Dollings findings, that nose tip bluntness would affect Magnus results. Results of the present investigation show that Magnus results are affected by nose tip bluntness.

SOCBT

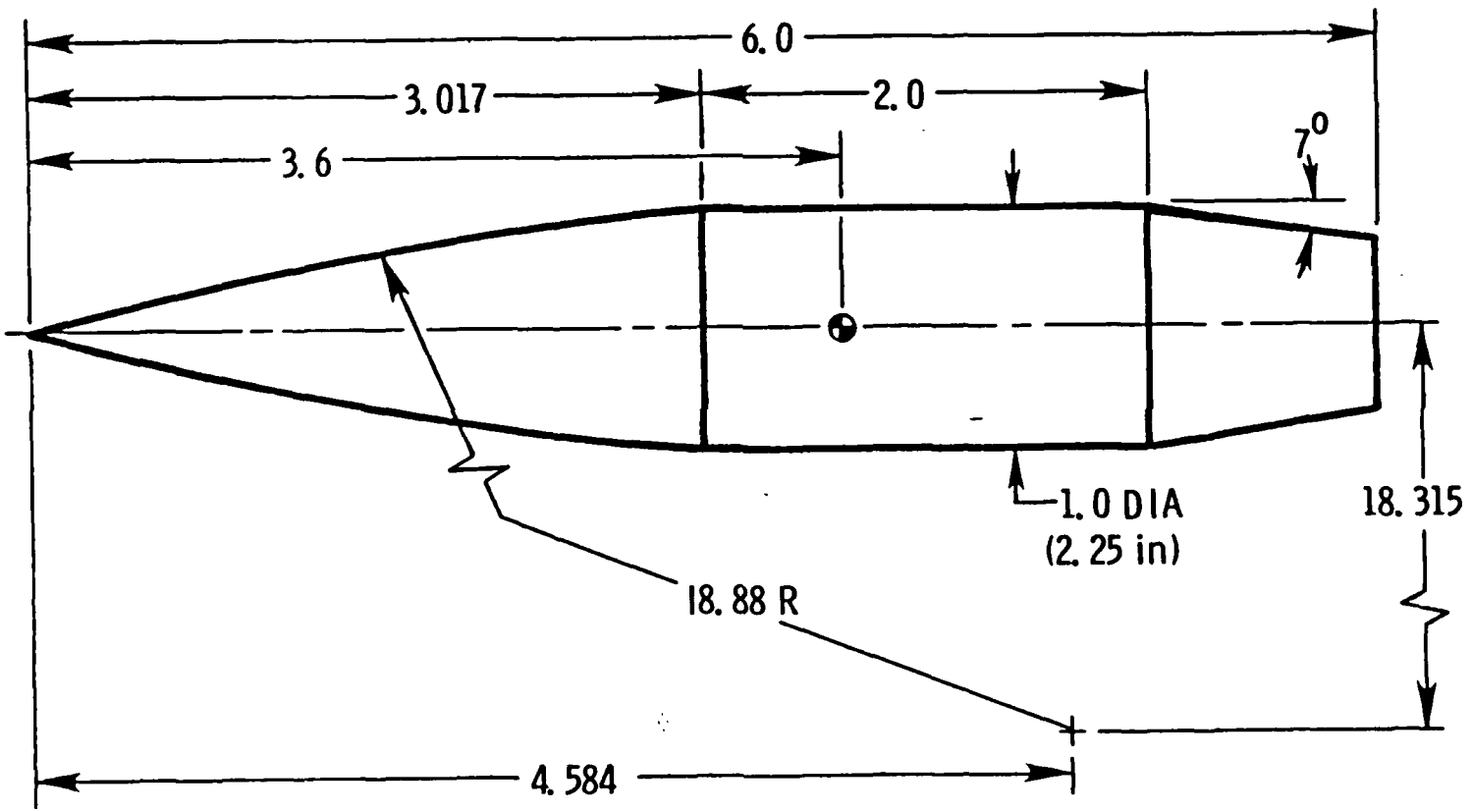

ALL DIMENSIONS IN CALIBERS

Figure 1. Model geometry, SOCBT.

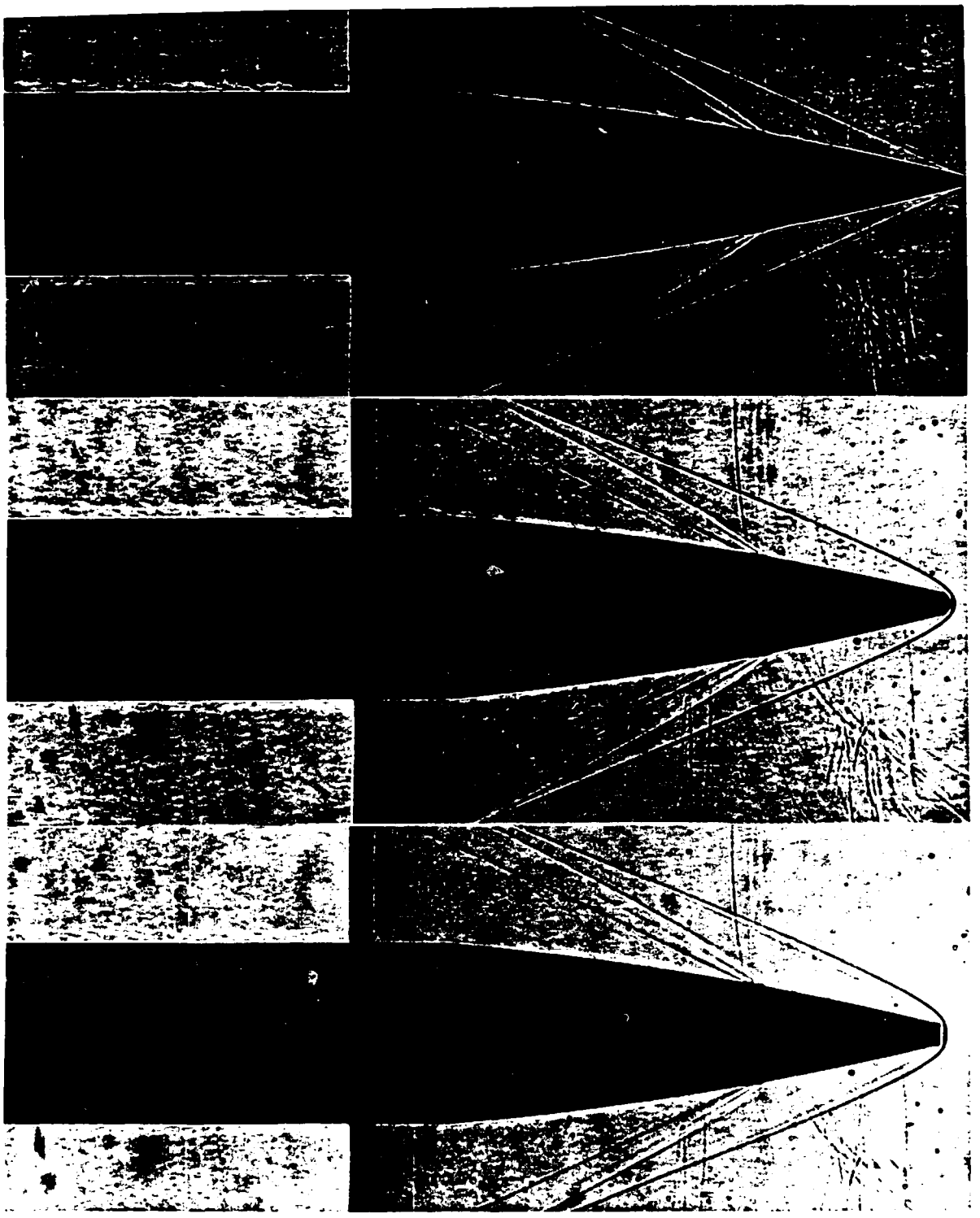

Figure 2. Shadowgraphs showing flat, spherical and sharp nose tips.

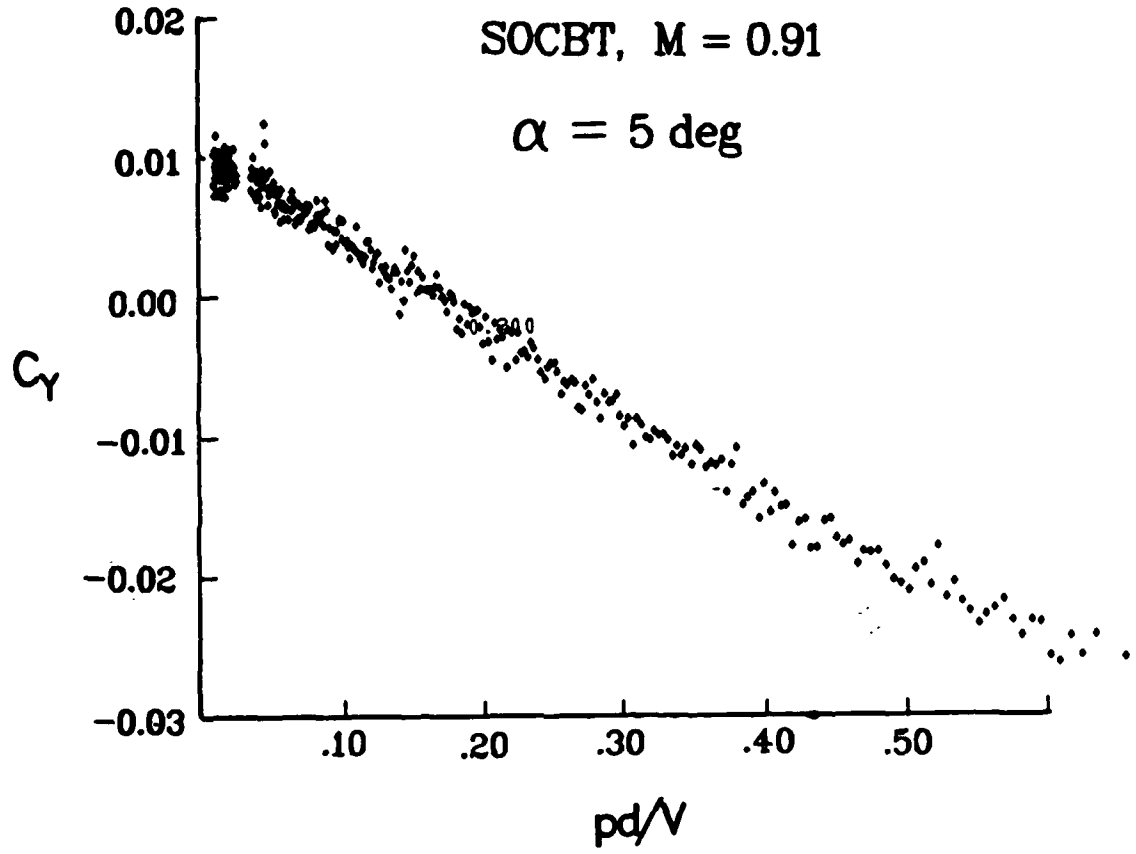

Figure 3. Typical side force data.

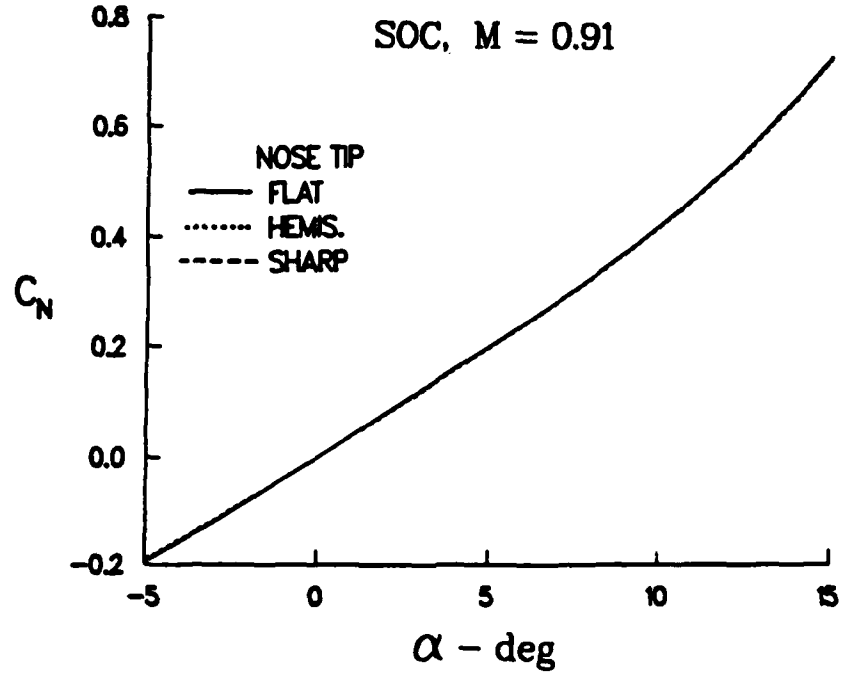

Figure 4a. C_N vs α, SOC, M = 0.91.

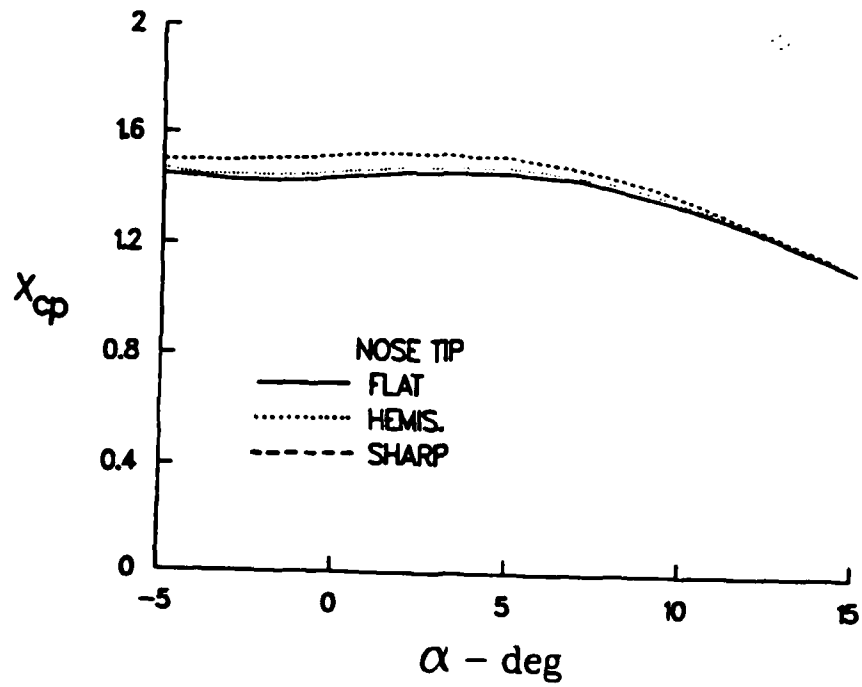

Figure 4b. X_{cp} vs α, SOCBT, M = 0.91.

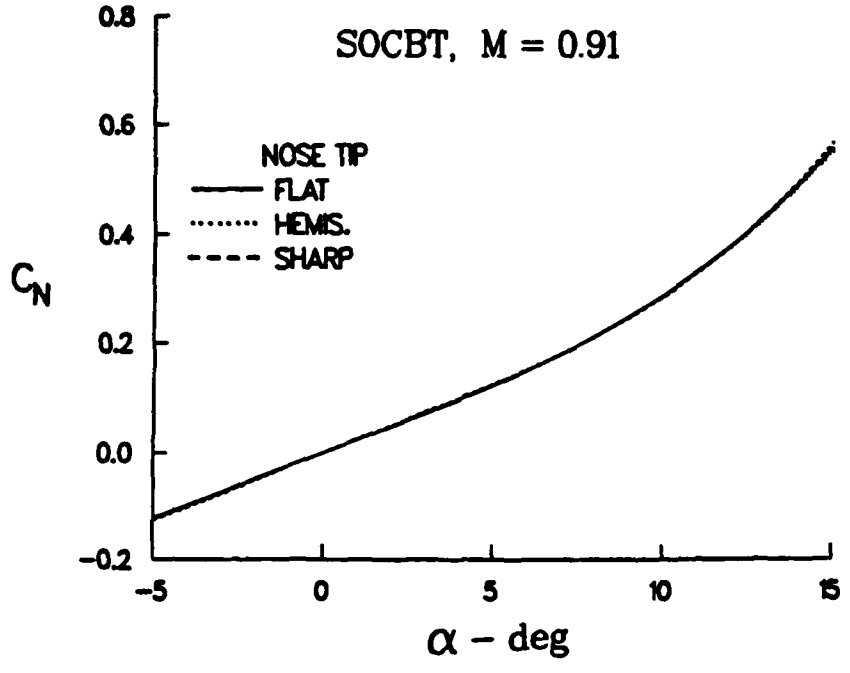

Figure 5a. C_N vs α, SOC, M = 0.91.

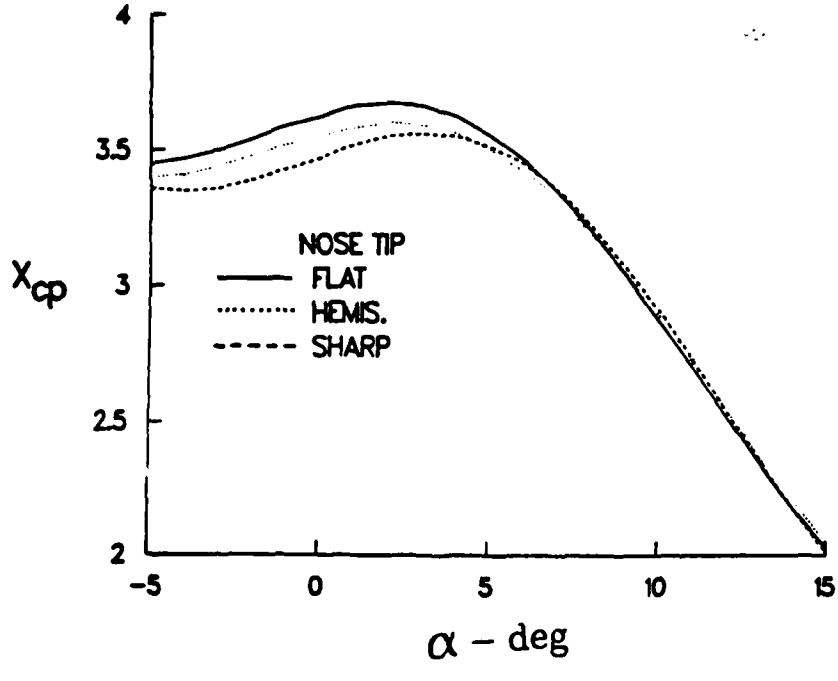

Figure 5b. X_{cp} vs α, SOCBT, M = 0.91.

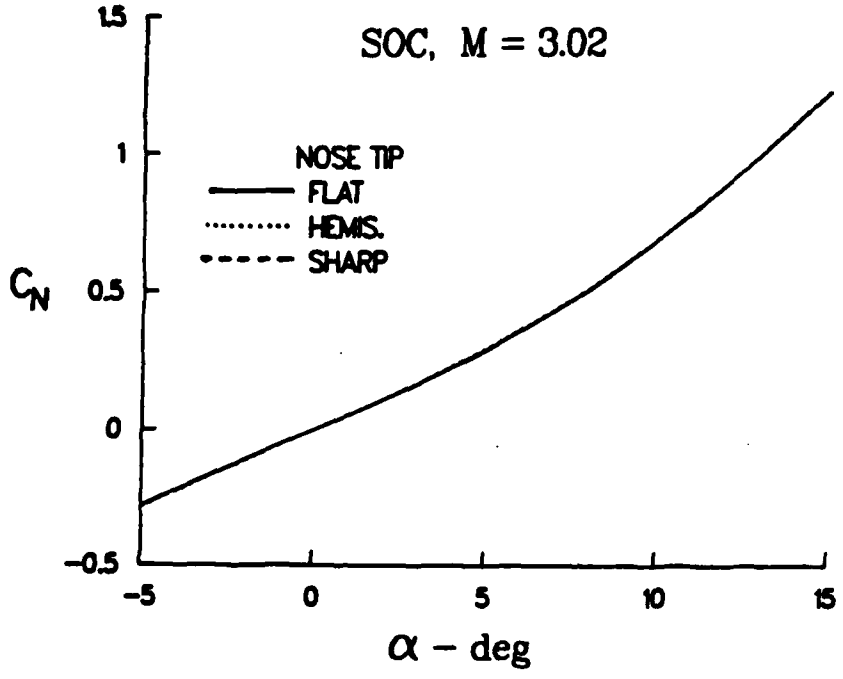

Figure 6a. C_N vs α, SOC, M = 3.02.

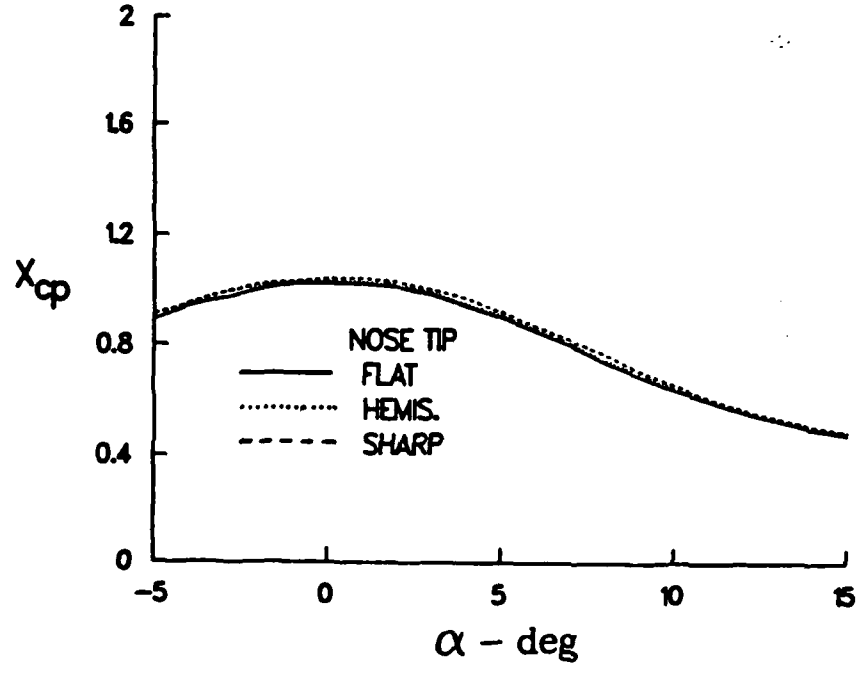

Figure 6b. X_{cp} vs α, SOCBT, M = 3.02.

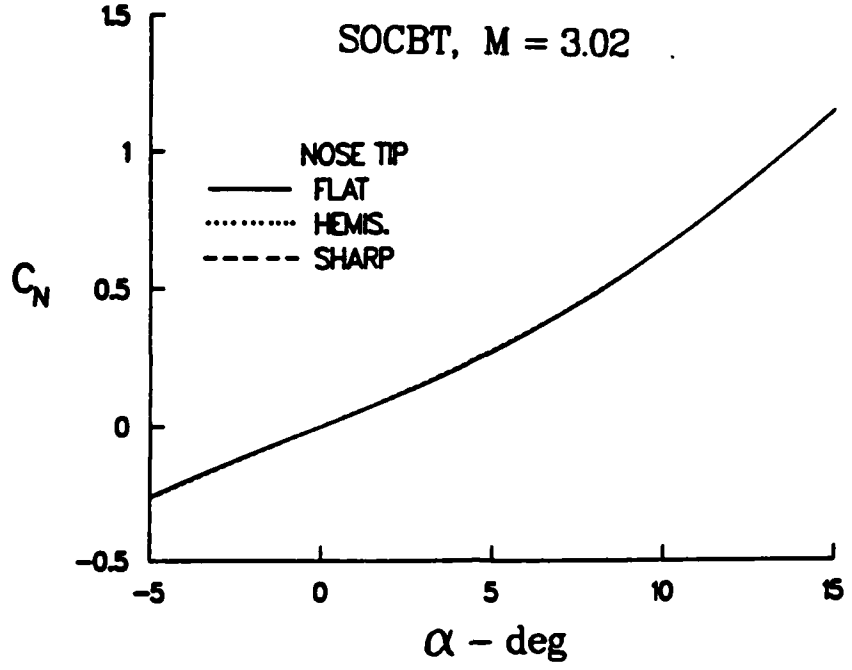

Figure 7a. C_N vs α, SOC, M = 3.02.

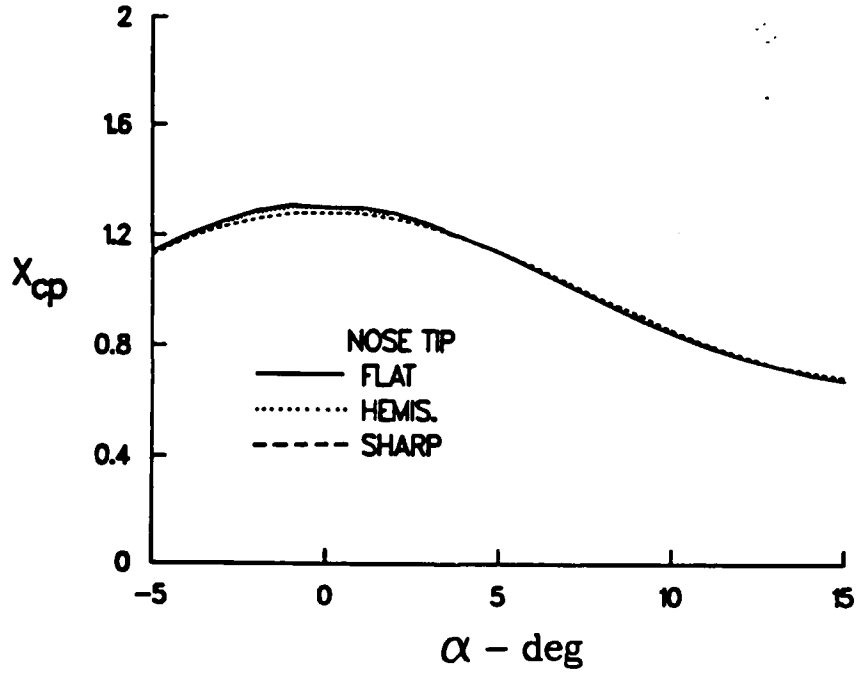

Figure 7b. X_{cp} vs α, SOCBT, M = 3.02.

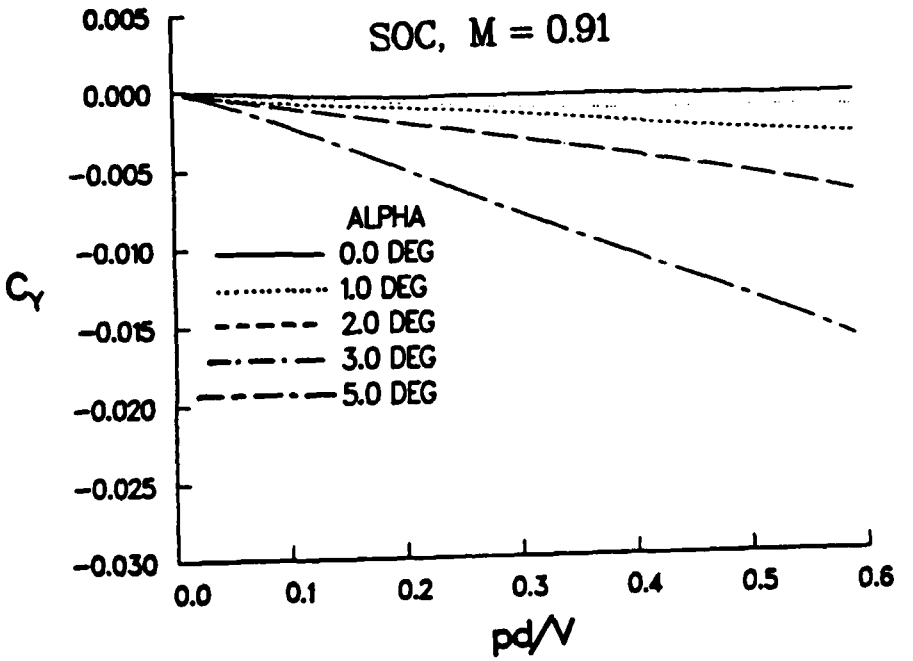

Figure 8a. Angle of attack effect on C_Y, SOC = 0.91, sharp nose tip.

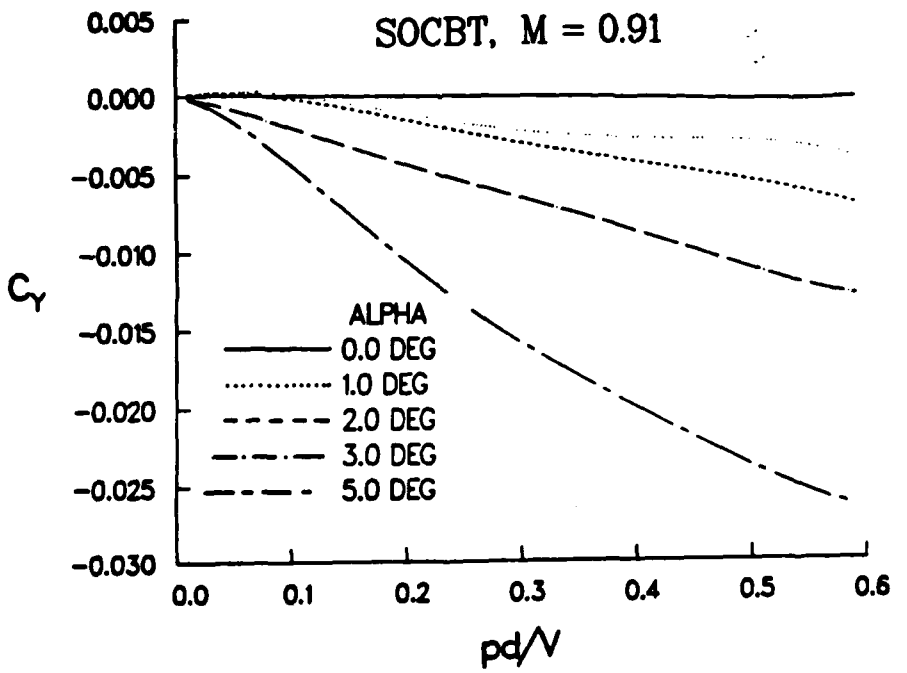

Figure 8b. Angle of attack effect on C_Y, SOCBT = 0.91, sharp nose tip.

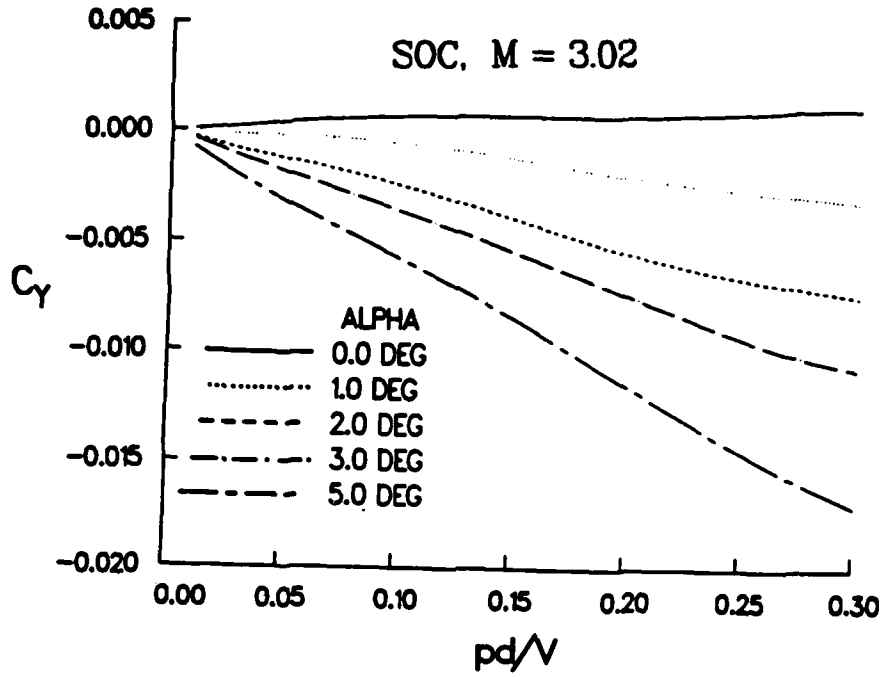

Figure 9a. Angle of attack effect on C_Y, SOC = 3.02, sharp nose tip.

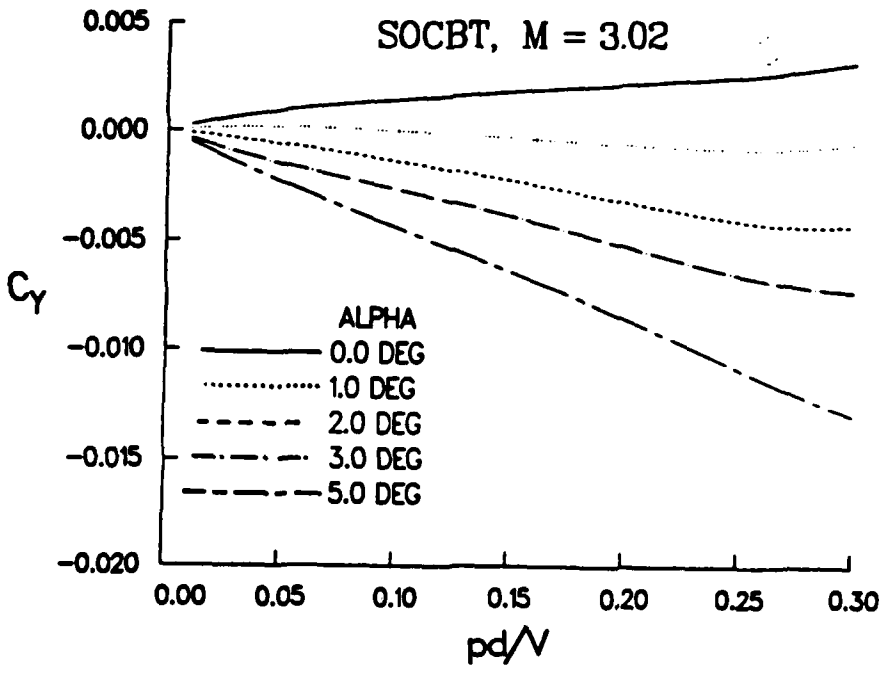

Figure 9b. Angle of attack effect on C_Y, SOCBT = 3.02, sharp nose tip.

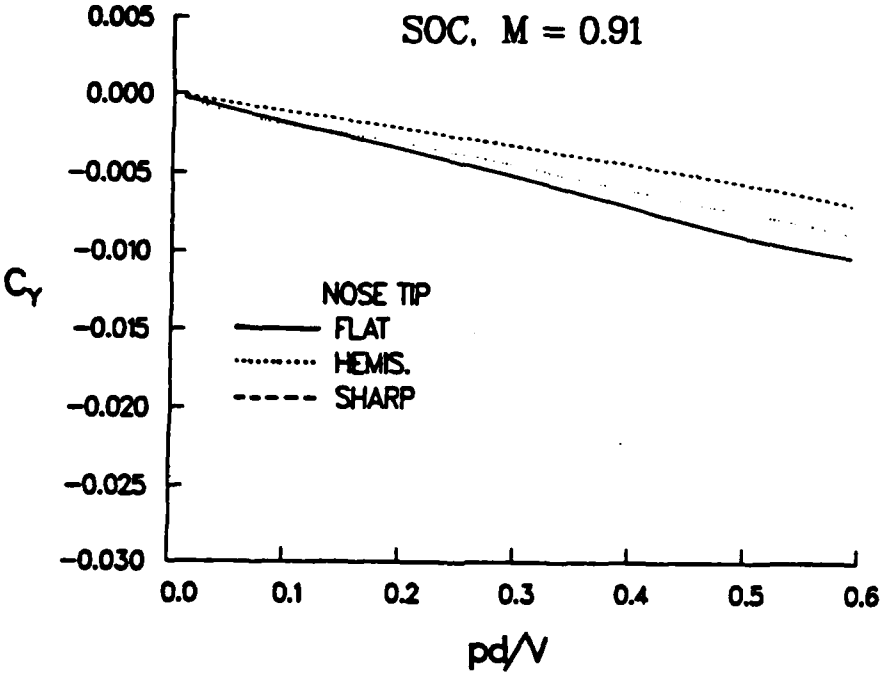

Figure 10a. Nose bluntness effect on C_Y, SOC = 0.91, α = 3°.

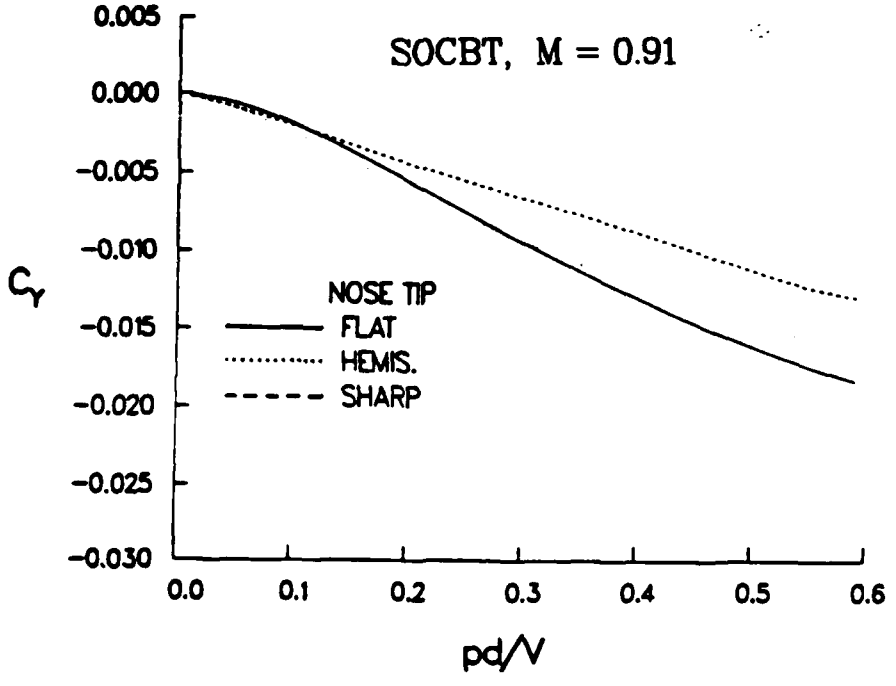

Figure 10b. Nose bluntness effect on C_Y, SOCBT = 0.91, α = 3°.

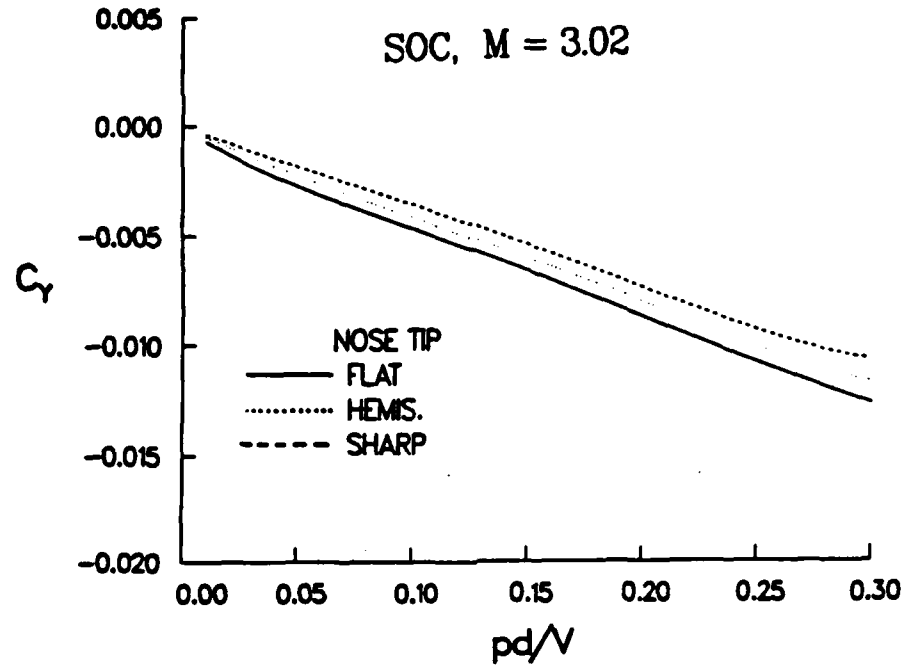

Figure 11a. Nose bluntness effect on C_Y, SOC = 3.02, α = 3°.

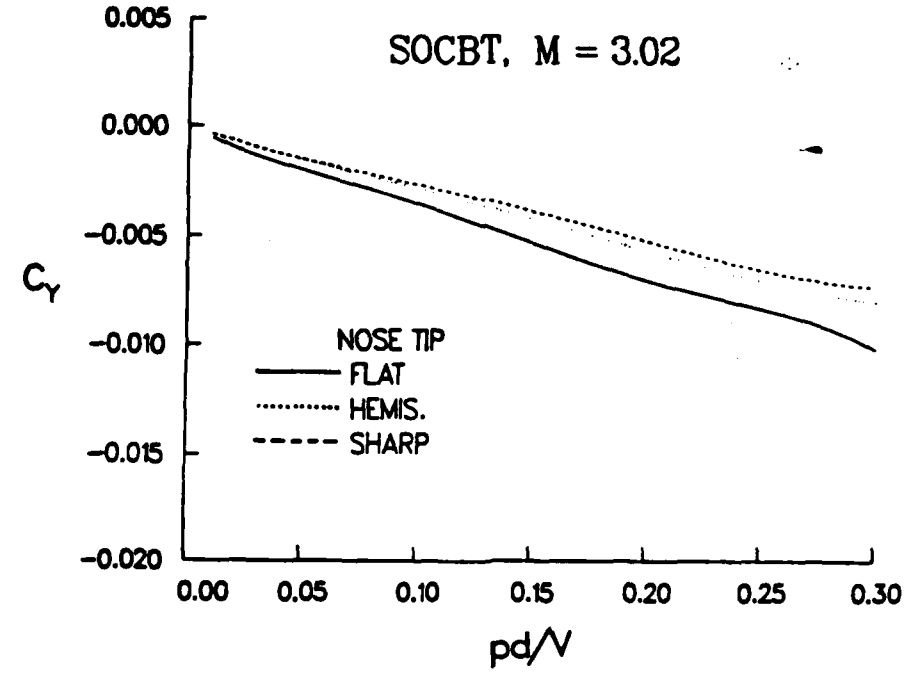

Figure 11b. Nose bluntness effect on C_Y, SOCBT = 3.02, α = 3°.

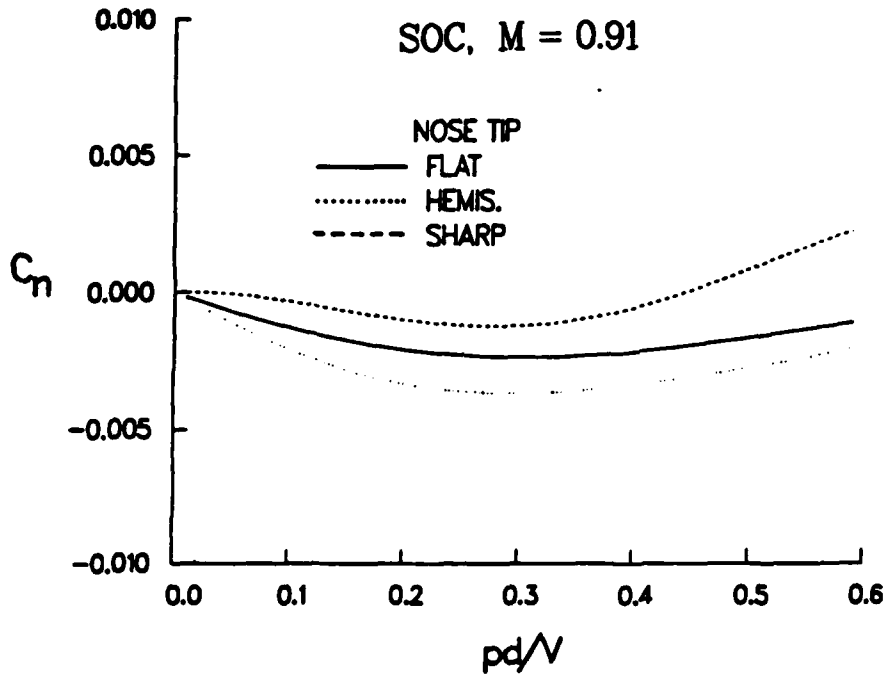

Figure 12a. Nose bluntness effect on C_n, SOC = 0.91, α = 3°.

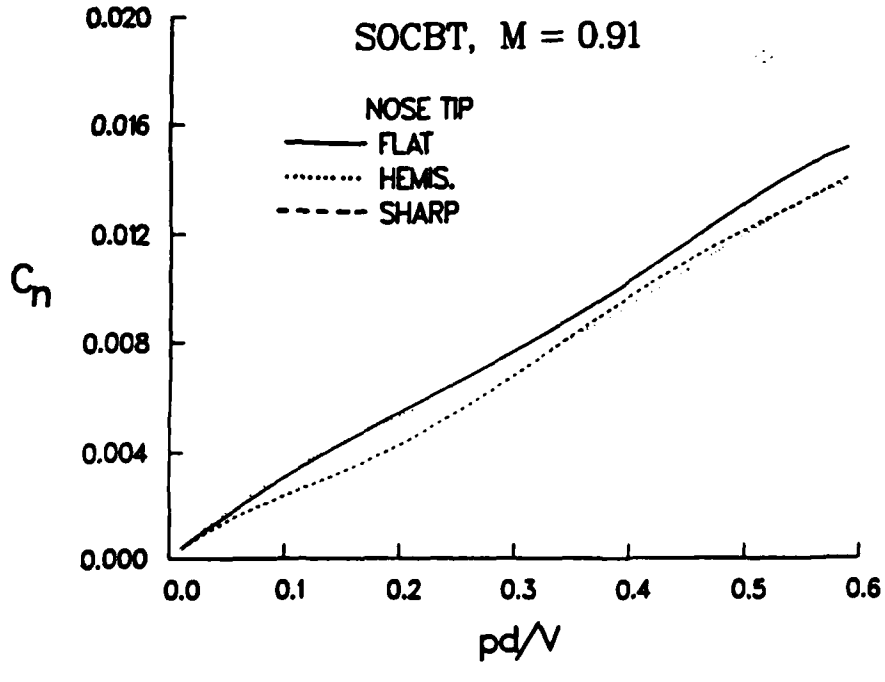

Figure 12b. Nose bluntness effect on C_n, SOCBT = 0.91, α = 3°.

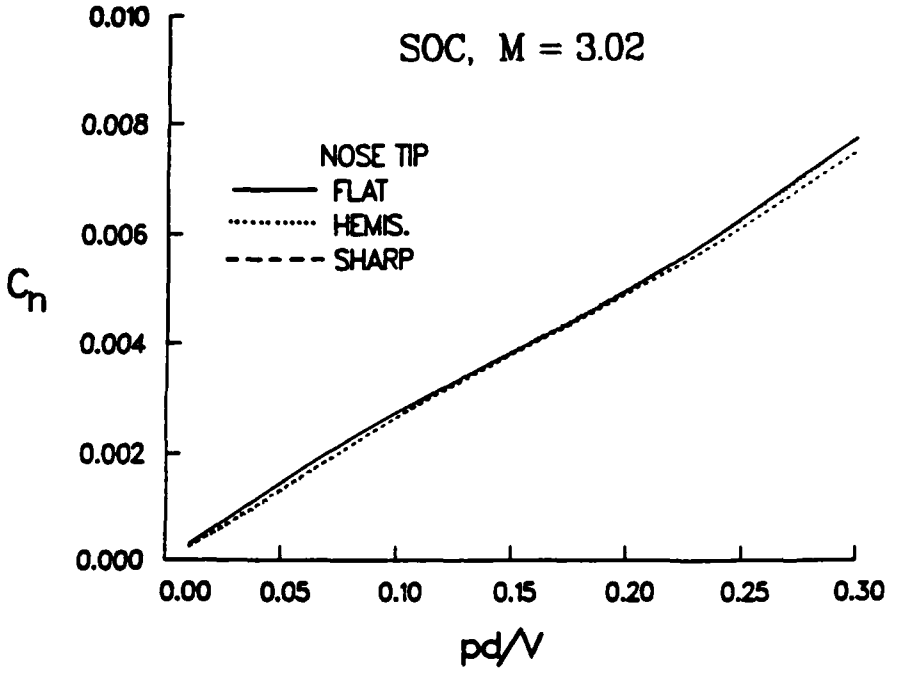

Figure 13a. Nose bluntness effect on C_n, SOC = 3.02, α = 3°.

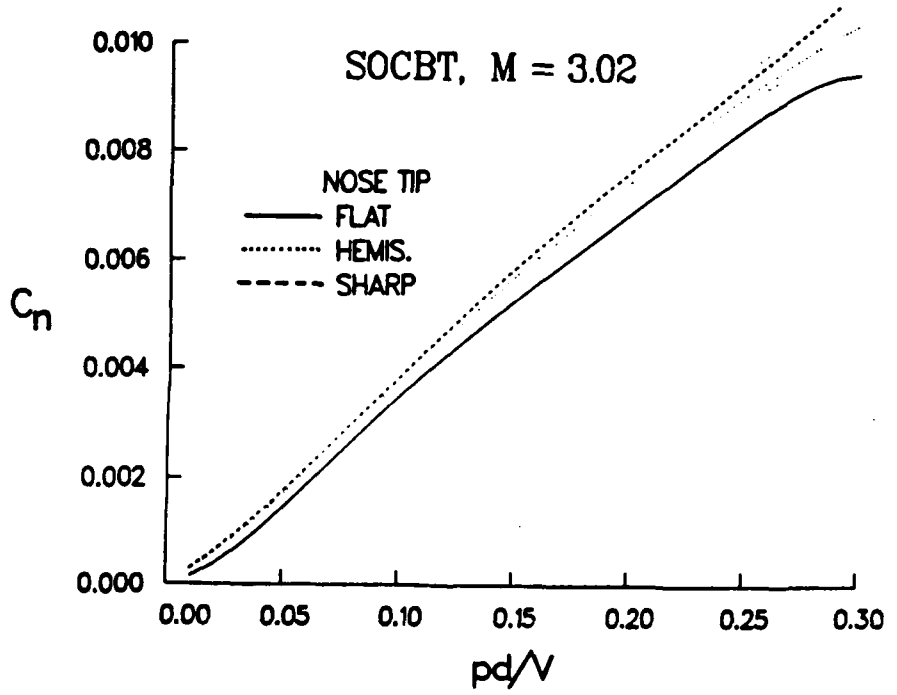

Figure 13b. Nose bluntness effect on C_n, SOCBT = 3.02, α = 3°.

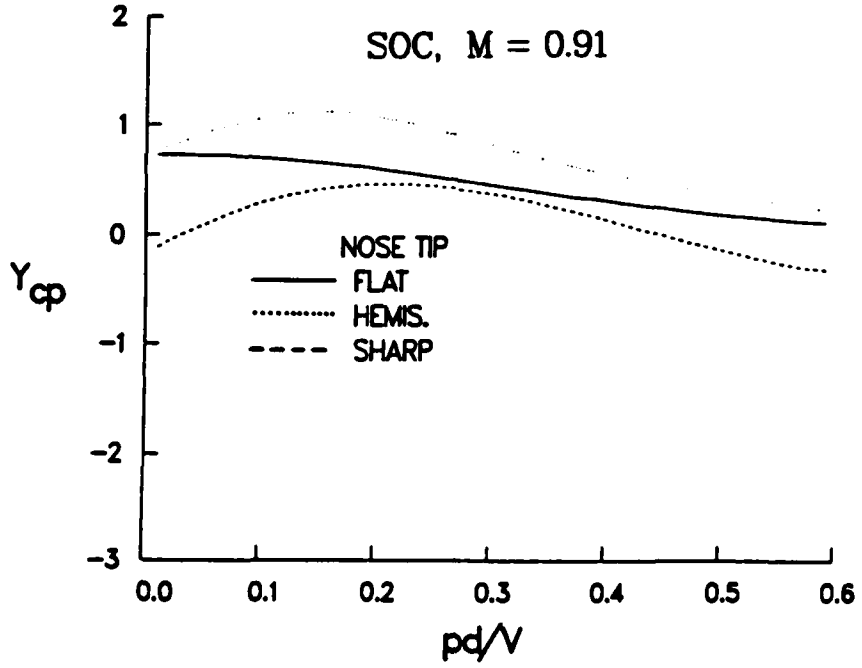

Figure 14a. Nose bluntness effect on Y_{cp}, SOC = 0.91, α = 3°.

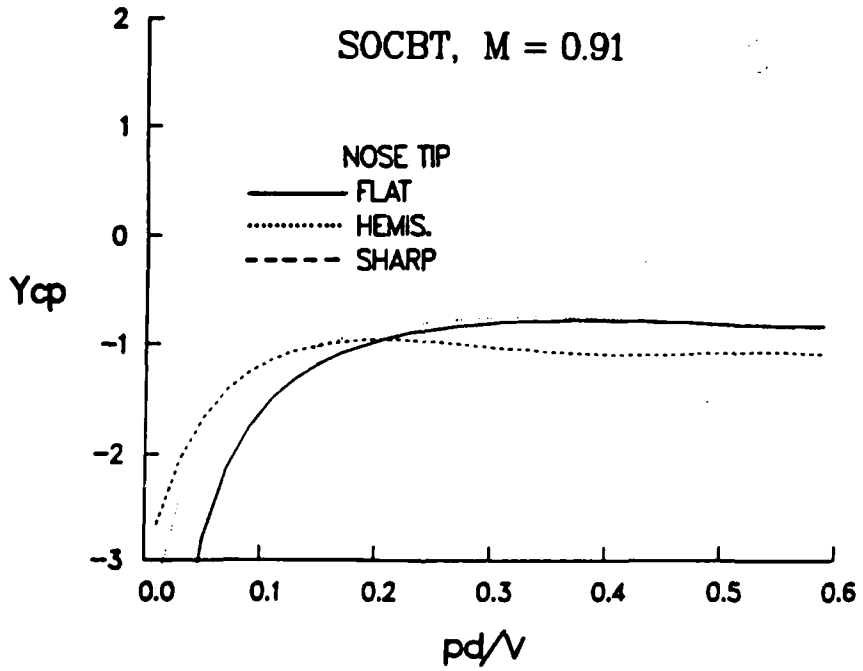

Figure 14b. Nose bluntness effect on Y_{cp}, SOCBT = 0.91, α = 3°.

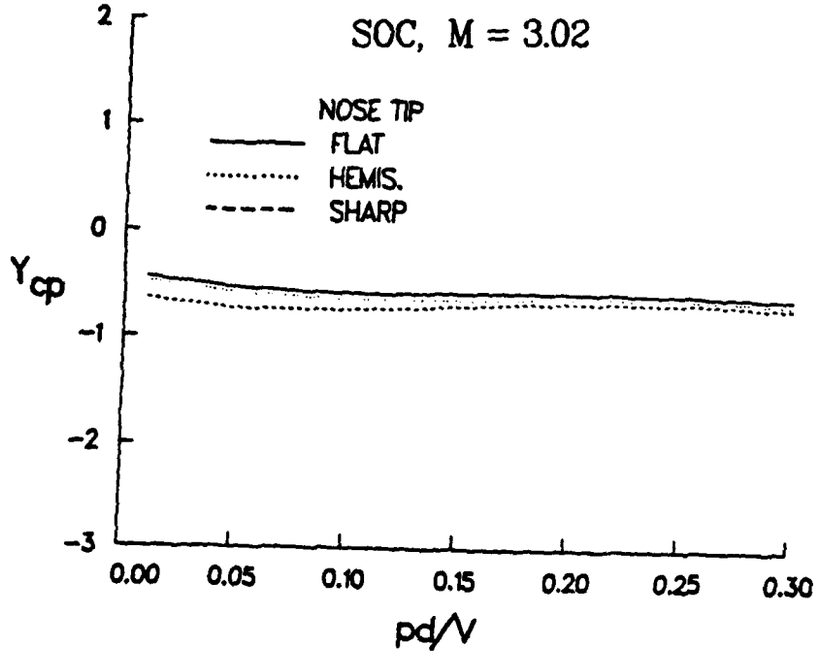

Figure 15a. Nose bluntness effect on Y_{cp}, SOC = 3.02, α = 3°.

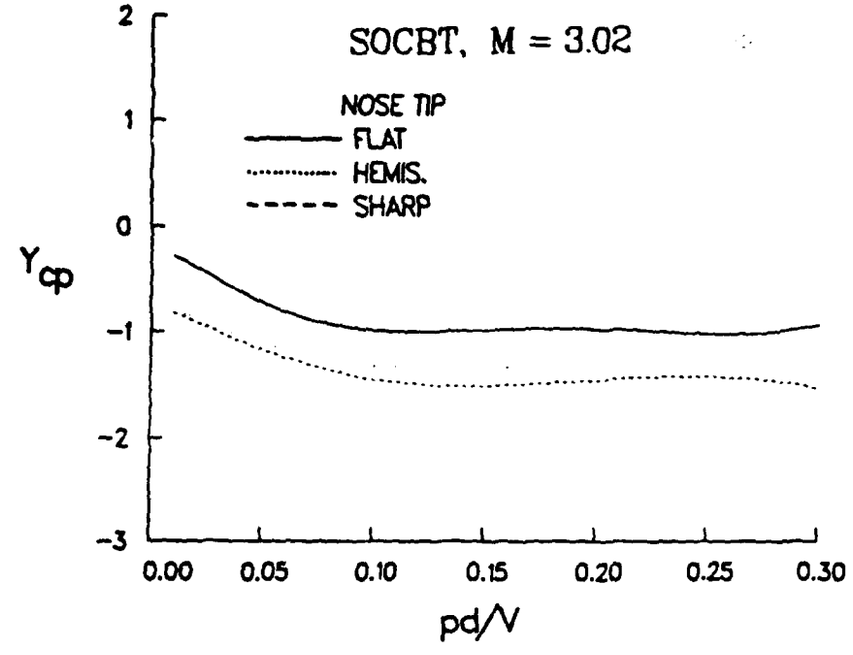

Figure 15b. Nose bluntness effect on Y_{cp}, SOCBT = 3.02, α = 3°.

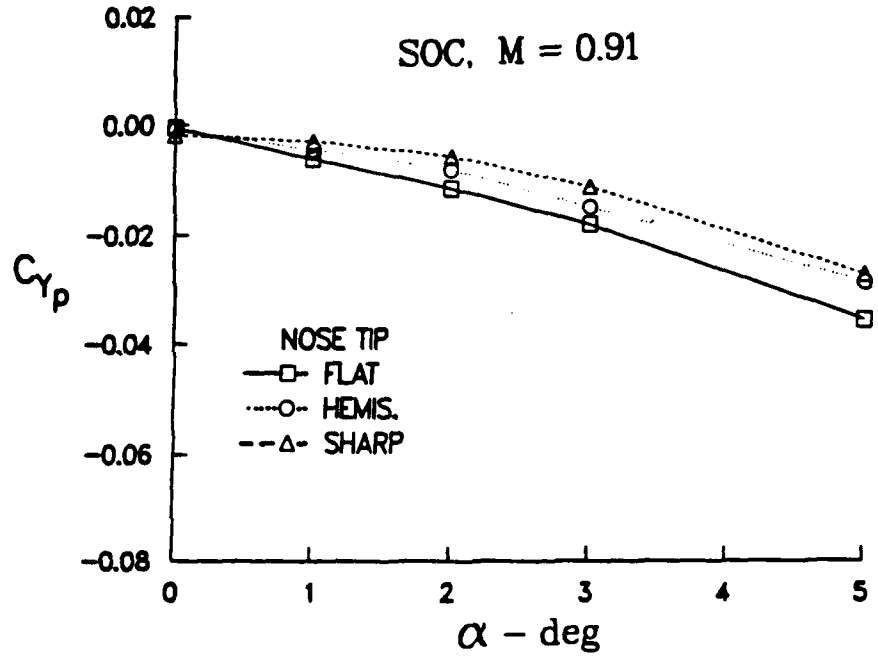

Figure 16a. Magnus force coefficients, SOC = 0.91.

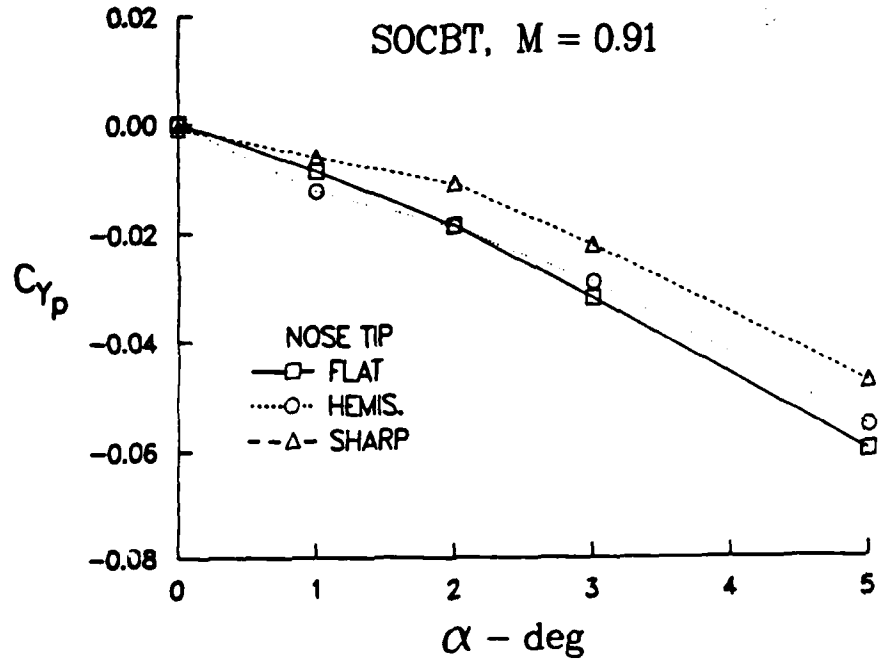

Figure 16b. Magnus force coefficients, SOCBT = 0.91.

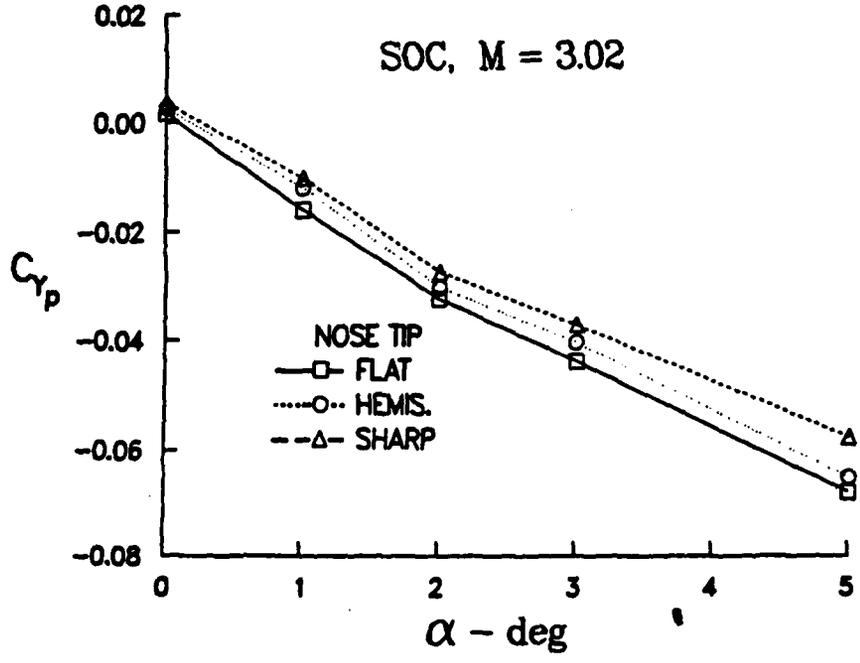

Figure 17a. Magnus force coefficients, SOC = 3.02.

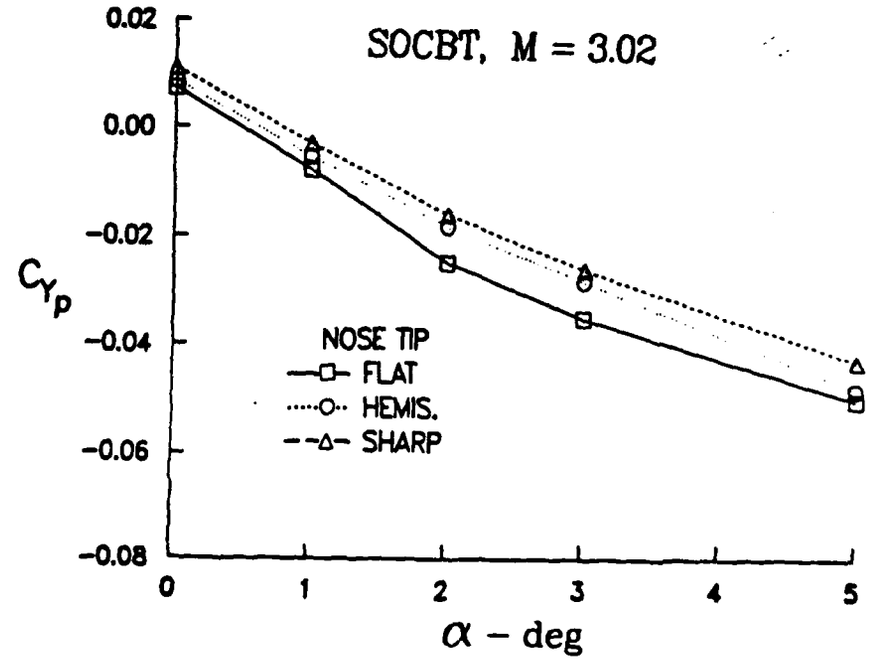

Figure 17b. Magnus force coefficients, SOCBT = 3.02.

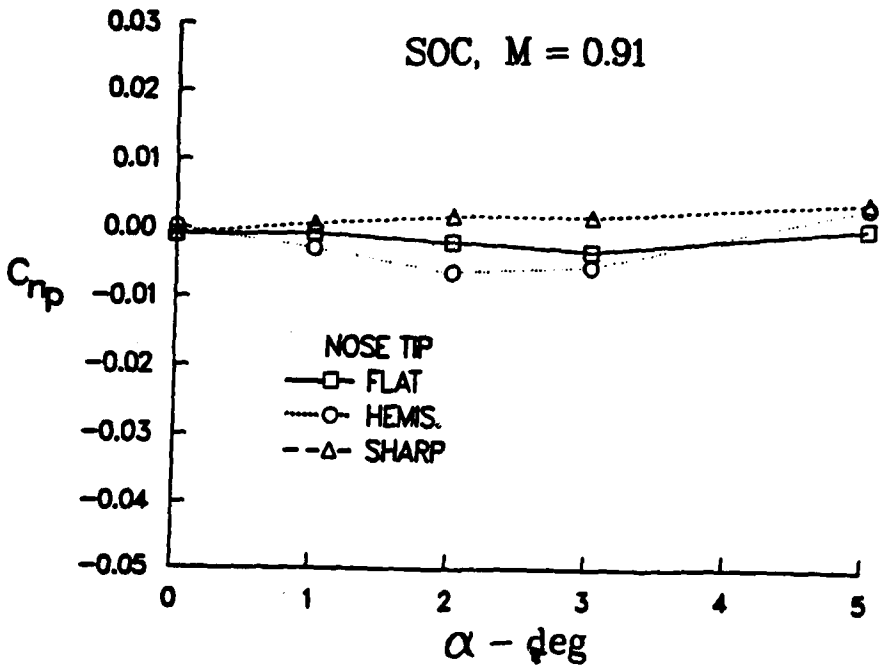

Figure 18a. Magnus force coefficients, SOC = 0.91.

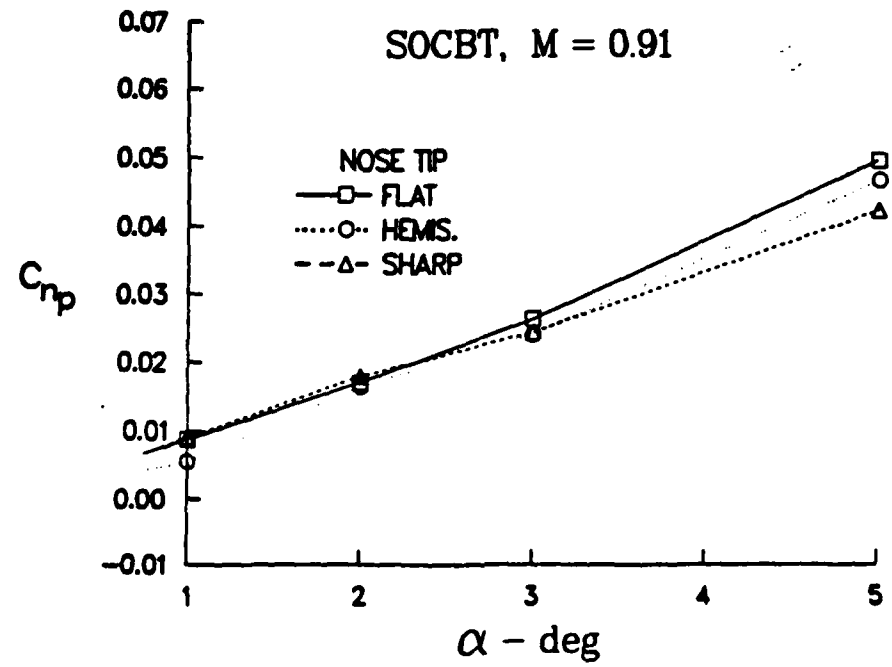

Figure 18b. Magnus force coefficients, SOCBT = 0.91.

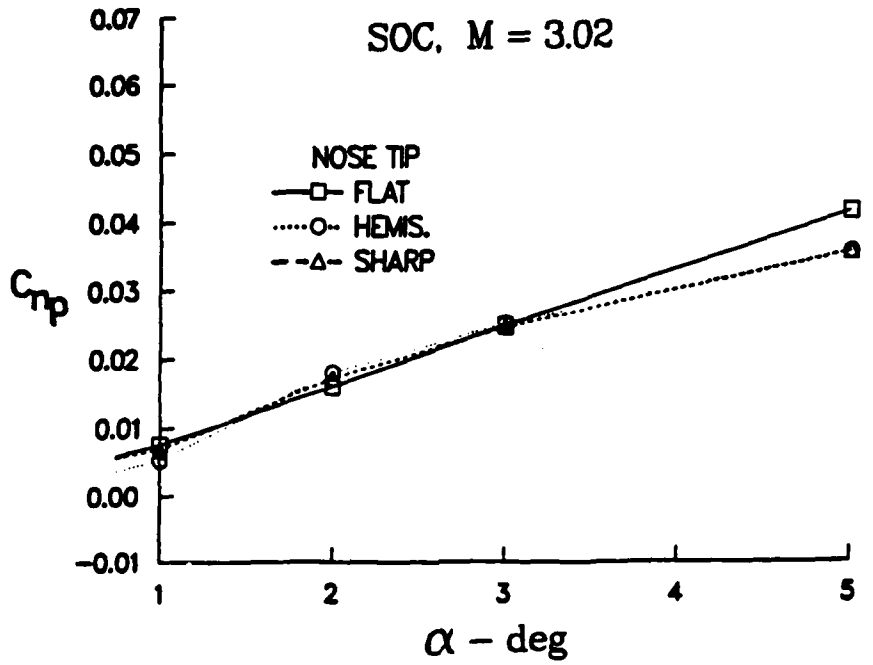

Figure 19a. Magnus force coefficients, SOC = 3.02.

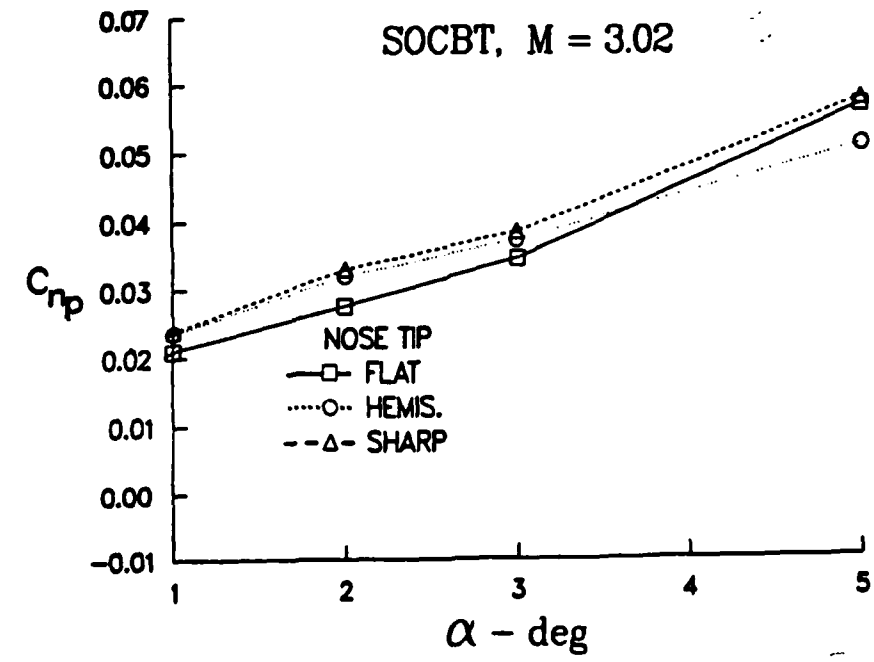

Figure 19b. Magnus force coefficients, SOCBT = 3.02.

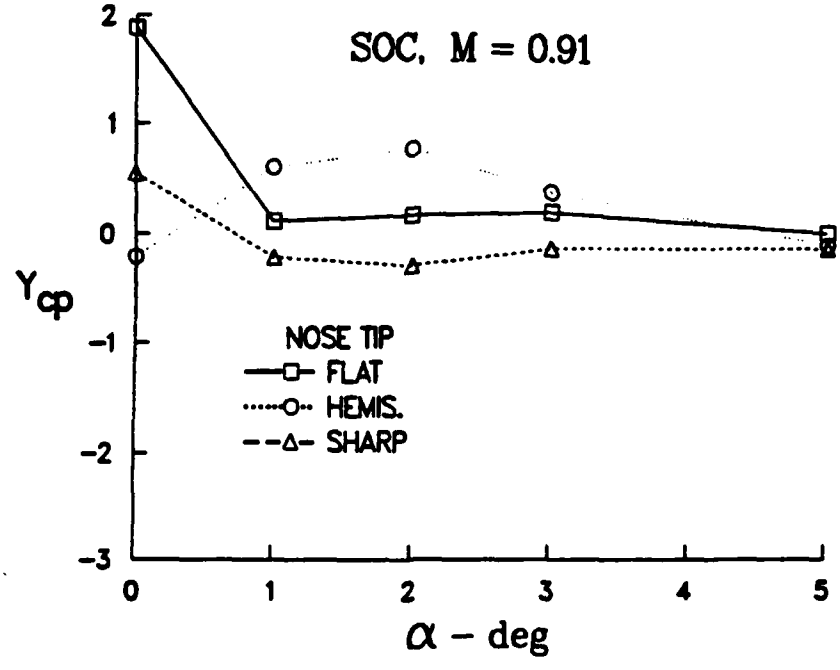

Figure 20a. Magnus center of pressure, SOC = 0.91.

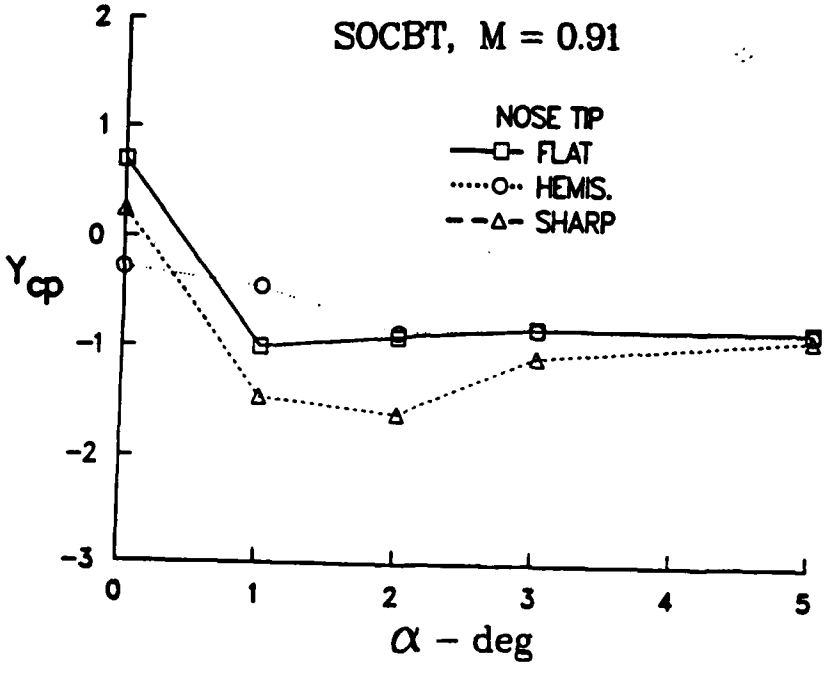

Figure 20b. Magnus center of pressure, SOCBT = 0.91.

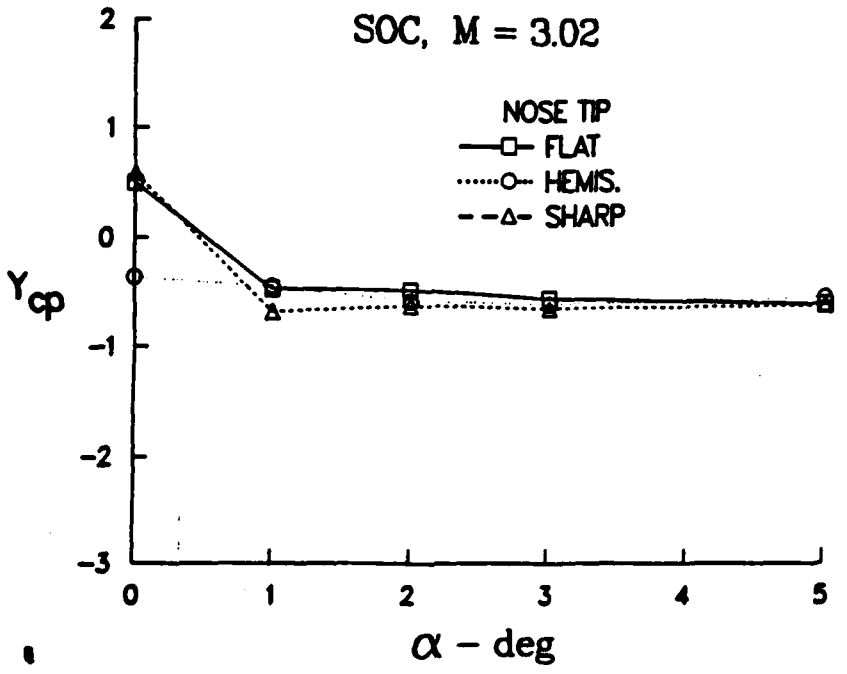

Figure 21a. Magnus center of pressure, SOC = 3.02.

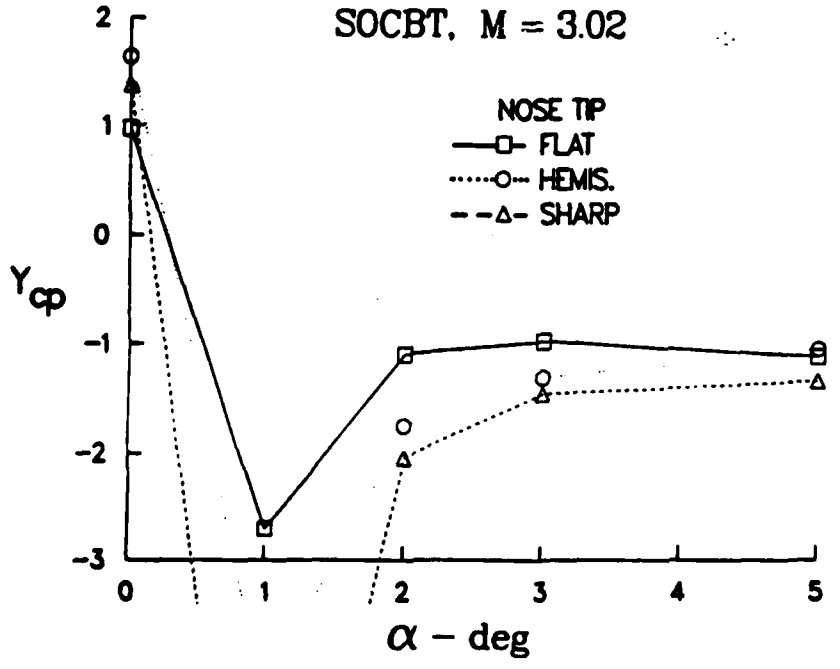

Figure 21b. Magnus center of pressure, SOCBT = 3.02.

TABLE 1. Polynomial Coefficient Data, SOC Side Force

NOSE	a1	a2	a3	a4	a5
M = 0.91, α = 0					
Flat	.2210e-02	-.3089e-01	.8241e-01	-.5741e-01	-.1077e-01
Hemis	.1154e-01	-.2110e-00	.9604e-00	-.1697e+01	.1041e+01
Sharp	-.1551e-02	-.3602e-01	.2264e-00	-.4753e-00	.3343e-00
M = 0.91, α = 1					
Flat	-.2024e-01	.1333e-00	-.4938e-00	.7950e-00	-.4576e-00
Hemis	-.1240e-02	-.7870e-01	.3536e-00	-.5944e-00	.3494e-00
Sharp	-.4909e-02	.3233e-02	-.4603e-01	.1735e-00	-.1596e-00
M = 0.91, α = 2					
Flat	-.1800e-01	.3579e-01	.4690e-01	-.3881e-00	.4032e-00
Hemis	.2954e-02	-.1141e-00	.4808e-00	-.9035e-00	.6159e-00
Sharp	-.1317e-01	.6893e-01	-.2374e-00	.3438e-00	-.1734e-00
M = 0.91, α = 3					
Flat	-.2051e-01	.2673e-01	-.6943e-01	.2210e-01	.5686e-01
Hemis	-.3175e-01	.1793e-00	-.7047e-00	.1184e+01	-.7173e-00
Sharp	-.1211e-01	.1281e-01	-.5920e-01	.1146e-00	-.8408e-01
M = 0.91, α = 5					
Flat	-.2673e-01	-.1143e-00	.4722e-00	-.7964e-00	.4781e-00
Hemis	-.2318e-02	-.3585e-00	.1563e+01	-.2774e+01	.1744e+01
Sharp	-.1696e-01	-.7539e-01	.1922e-00	-.1852e-00	.4159e-01
M = 3.02, α = 0					
Flat	-.8279e-02	.2699e-00	-.2149e+01	.6648e+01	-.7003e+01
Hemis	.4050e-02	.8257e-01	-.9462e-00	.3109e+01	-.3047e+01
Sharp	.4772e-02	.1309e-00	-.1777e+01	.7507e+01	-.1023e+02
M = 3.02, α = 1					
Flat	-.4042e-01	.6716e-00	-.5625e+01	.1875e+02	-.2176e+02
Hemis	-.8404e-02	.1362e-00	-.1674e+01	.5690e+01	-.5780e+01
Sharp	-.9174e-02	.1947e-00	-.2389e+01	.9358e+01	-.1199e+02
M = 3.02, α =2					
Flat	-.8438e-01	.1125e+01	-.8636e+01	.2812e+02	-.3273e+02
Hemis	-.5319e-01	.5257e-00	-.4075e+01	.1299e+02	-.1440e+02
Sharp	-.3474e-01	.3325e-00	-.3425e+01	.1300e+02	-.1634e+02
M = 3.02, α = 3					
Flat	-.7342e-01	.5092e-00	-.3286e+01	.9330e+01	-.9606e+01
Hemis	-.4944e-01	.9287e-01	-.1815e-01	-.2099e+01	.5043e+01
Sharp	-.4000e-01	.8318e-01	-.4901e-00	.4539e-00	.1387e+01
M = 3.02, α = 5					
Flat	-.9557e-01	.5103e-00	-.3390e+01	.9551e+01	-.9429e+01
Hemis	-.9387e-01	.5357e-00	-.3755e+01	.1162e+02	-.1310e+02
Sharp	-.7945e-01	.4564e-00	-.3161e+01	.8762e+01	-.8174e+01

TABLE 2. Polynomial Coefficient Data, SOC Yawing Moment

NOSE	b1	b2	b3	b4	b5
M = 0.91, α = 0					
Flat	-.1136e-01	.8748e-01	-.2567e-00	.2904e-00	-.8597e-01
Hemis	-.9191e-02	.1043e-00	-.4963e-00	.9946e-00	-.6866e-00
Sharp	.2612e-02	-.6622e-01	.3004e-00	-.5242e-00	.3241e-00
M = 0.91, α = 1					
Flat	.7342e-02	-.1026e-00	.3395e-00	-.3925e-00	.1289e-00
Hemis	-.6327e-02	-.2841e-01	.4269e-01	.2191e-00	-.3188e-00
Sharp	-.9435e-02	.9739e-01	-.4710e-00	.9614e-00	-.6513e-00
M = 0.91, α = 2					
Flat	-.4768e-03	-.9937e-01	.5553e-00	-.1063e+01	.6944e-00
Hemis	-.2044e-01	.1835e-01	.3456e-01	.6555e-02	-.5927e-01
Sharp	.1114e-01	-.1978e-00	.8505e-00	-.1385e+01	.8097e-00
M = 0.91, α = 3					
Flat	-.1294e-01	.1602e-01	.3090e-01	-.2410e-01	-.2015e-01
Hemis	-.1996e-01	-.1056e-01	.2633e-00	-.5159e-00	.3182e-00
Sharp	.3277e-02	-.7444e-01	.2143e-00	-.9704e-01	-.7446e-01
M = 0.91, α = 5					
Flat	-.5257e-01	.5932e-00	-.2256e+01	.3632e+01	-.2083e+01
Hemis	.1883e-01	-.3822e-00	.1929e+01	-.3576e+01	.2292e+01
Sharp	-.6464e-01	.5036e-00	-.1624e+01	.2569e+01	-.1527e+01
M = 3.02, α = 0					
Flat	-.2477e-02	.2240e-01	.1070e-00	-.1208e+01	.2545e+01
Hemis	-.7559e-02	.1435e-00	-.1345e+01	.5419e+01	-.7458e+01
Sharp	.7206e-03	.9409e-01	-.1021e+01	.3738e+01	-.4293e+01
M = 3.02, α = 1					
Flat	.2766e-01	-.5445e-00	.4718e+01	-.1635e+02	.2028e+02
Hemis	-.8102e-02	.1008e-00	.4566e-01	-.1565e+01	.3210e+01
Sharp	-.1149e-02	-.5459e-01	.1649e+01	-.8374e+01	.1314e+02
M = 3.02, α = 2					
Flat	.4637e-01	-.4054e-00	.1949e+01	-.3172e+01	.8050e-00
Hemis	.2313e-01	.7845e-01	-.1353e+01	.6419e+01	-.9438e+01
Sharp	.1071e-01	.2658e-00	-.2577e+01	.1011e+02	-.1360e+02
M = 3.02, α = 3					
Flat	.3707e-01	-.2147e-01	-.5699e-00	.3467e+01	-.5286e+01
Hemis	.2675e-01	.1310e-00	-.1316e+01	.4699e+01	-.5504e+01
Sharp	.2820e-01	.9501e-01	-.1150e+01	.4567e+01	-.5907e+01
M = 3.02, α = 5					
Flat	.5625e-01	.3096e-01	-.1124e+01	.5439e+01	-.7885e+01
Hemis	.5902e-01	-.2502e-00	.1211e+01	-.1995e+01	.4639e-00
Sharp	.4290e-01	.1115e-00	-.1831e+01	.8965e+01	-.1393e+02

cg is 2.5 cal. from base

TABLE 3. Polynomial Coefficient Data, SOCBT Side Force

NOSE	a1	a2	a3	a4	a5
M = 0.91, α = 0					
Flat	.8952e-02	-.9920e-01	.3126e-00	-.3176e-00	.5454e-01
Hemis	-.4668e-02	.2388e-01	-.7254e-01	.1065e-00	-.5932e-01
Sharp	.2089e-02	-.3633e-01	.1724e-00	-.3491e-00	.2520e-00
M = 0.91, α = 1					
Flat	.2213e-01	-.3623e-00	.1545e+01	-.2758e+01	.1741e+01
Hemis	-.3555e-01	.2273e-00	-.9447e-00	.1705e+01	-.1079e+01
Sharp	.1413e-01	-.1802e-00	.4675e-00	-.3736e-00	-.6093e-02
M = 0.91, α = 2					
Flat	-.2043e-02	-.1126e-00	.3054e-00	-.3802e-00	.1699e-00
Hemis	-.7713e-02	-.5570e-01	.4441e-02	.2406e-00	-.2351e-00
Sharp	.1064e-01	-.1690e-00	.4777e-00	-.5653e-00	.2220e-00
M = 0.91, α = 3					
Flat	-.2039e-02	-.2295e-00	.6494e-00	-.8461e-00	.4473e-00
Hemis	-.9904e-02	-.2146e-00	.7583e-00	-.1131e+01	.6371e-00
Sharp	-.1199e-01	-.1343e-00	.6175e-00	-.1185e+01	.8069e-00
M = 0.91, α = 5					
Flat	-.4782e-01	-.1264e-00	.3893e-00	-.5153e-00	.2893e-00
Hemis	-.3333e-01	-.3744e-00	.1474e+01	-.2255e+01	.1252e+01
Sharp	-.1454e-01	-.4389e-00	.1712e+01	-.2736e+01	.1607e+01
M = 3.02, α = 0					
Flat	.2933e-01	-.5107e-00	.4628e+01	-.1862e+02	.2732e+02
Hemis	.1611e-01	-.6803e-01	.2388e-00	-.8354e-00	.1885e+01
Sharp	.2740e-01	-.2466e-00	.1565e+01	-.5039e+01	.6490e+01
M=3.02, α =1					
Flat	.8118e-02	-.2864e-01	-.1146e+01	.5837e+01	-.6878e+01
Hemis	.5257e-02	-.9823e-01	.2954e-00	-.6563e-00	.1451e+01
Sharp	.9117e-02	-.1545e-00	.8627e-00	-.2795e+01	.4130e+01
M = 3.02, α = 2					
Flat	-.4471e-01	.6366e-00	-.6501e+01	.2611e+02	-.3526e+02
Hemis	-.2141e-01	.1940e-00	-.1838e+01	.5860e+01	-.5613e+01
Sharp	-.8999e-02	-.9505e-01	.7630e-00	-.3617e+01	.6471e+01
M = 3.02, α = 3					
Flat	-.5982e-01	.6367e-00	-.5914e+01	.2301e+02	-.3137e+02
Hemis	-.3568e-01	.1432e-00	-.9254e-00	.2206e+01	-.1252e+01
Sharp	-.3787e-01	.2037e-00	-.1096e+01	.1745e+01	.5018e-00
M = 3.02, α = 5					
Flat	-.6726e-01	.2537e-00	-.1447e+01	.3863e+01	-.4124e+01
Hemis	-.6083e-01	.1227e-00	-.2061e-00	-.1155e+01	.3572e+01
Sharp	-.4955e-01	.5018e-01	.2908e-00	-.3031e+01	.5801e+01

TABLE 4. Polynomial Coefficient Data, SOCBT Yawing Moment

Nose	b1	b2	b3	b4	b5
M = 0.91, α = 0					
Flat	.1967e-02	-.7351e-01	.3274e-00	-.4764e-00	.2114e-00
Hemis	.8462e-02	-.1138e-00	.5605e-00	-.1097e+01	.7347e-00
Sharp	.7070e-02	-.1183e-00	.5584e-00	-.1036e+01	.6696e-00
M = 0.91, α = 1					
Flat	.2127e-01	-.2221e-00	.1087e+01	-.2014e+01	.1269e+01
Hemis	-.1215e-01	.1996e-00	-.8019e-00	.1382e+01	-.8504e-00
Sharp	.4028e-01	-.3307e-00	.1083e+01	-.1376e+01	.5761e-00
M = 0.91, α = 2					
Flat	.3536e-01	-.1856e-00	.7736e-00	-.1347e+01	.8214e-00
Hemis	.2807e-01	-.2966e-01	-.4704e-01	.2258e-00	-.1828e-00
Sharp	.4354e-01	-.2668e-00	.9558e-00	-.1400e+01	.7194e-00
M = 0.91, α = 3					
Flat	.3642e-01	-.3307e-01	-.4923e-01	.3626e-00	-.3753e-00
Hemis	.4166e-01	-.6985e-01	-.9035e-02	.3918e-00	-.4251e-00
Sharp	.3845e-01	-.1954e-00	.8752e-00	-.1517e+01	.9056e-00
M = 0.91, α = 5					
Flat	.6394e-01	-.3615e-02	-.1751e-00	.5276e-00	-.4615e-00
Hemis	.9907e-01	-.3668e-00	.1229e+01	-.1888e+01	.1044e+01
Sharp	.6017e-01	-.7099e-01	.2626e-00	-.5695e-00	.4449e-00
M = 3.02, α = 0					
Flat	.1615e-01	-.2656e-00	.3341e+01	-.1709e+02	.2888e+02
Hemis	.3622e-01	-.4356e-00	.3533e+01	-.1318e+02	.1742e+02
Sharp	.2730e-01	-.2260e-00	.2013e+01	-.8710e+01	.1296e+02
M = 3.02, α = 1					
Flat	.4034e-01	.5434e-02	-.1541e+01	.6856e+01	-.8046e+01
Hemis	.3040e-01	-.4561e-01	.4734e-00	-.3118e+01	.5553e+01
Sharp	.4252e-01	-.2915e-00	.2356e+01	-.9652e+01	.1436e+02
M = 3.02, α = 2					
Flat	.2656e-01	.1511e-00	-.1295e+01	.3840e+01	-.3570e+01
Hemis	.3406e-01	.5151e-01	-.1909e-00	-.9266e-00	.2737e+01
Sharp	.4148e-01	-.2008e-00	.2202e+01	-.9559e+01	.1345e+02
M = 3.02, α = 3					
Flat	.1469e-01	.5593e-00	-.4620e+01	.1615e+02	-.2072e+02
Hemis	.2741e-01	.2801e-00	-.2060e+01	.6376e+01	-.7513e+01
Sharp	.3100e-01	.2005e-00	-.1251e+01	.2872e+01	-.2039e+01
M = 3.02, α = 5					
Flat	.4310e-01	.5383e-00	-.4663e+01	.1631e+02	-.2086e+02
Hemis	.4994e-01	.4168e-00	-.4651e+01	.1836e+02	-.2418e+02
Sharp	.6699e-01	.7370e-02	-.8430e-01	-.1144e+01	.3552e+01

cg is 2.5 cal. from base

REFERENCE

1. Dolling, D.S. and Gray, W.K., "Experimental Study of Supersonic Turbulent Flow on a Blunted Axisymmetric Body," AIAA Journal, Volume 24, Number 5, May 1986, pp. 793-799.

LIST OF SYMBOLS

C_m = pitching moment coefficient, cg 2.4 cal from base

C_N = normal force coefficient

C_n = yawing moment coefficient, cg 2.4 cal. from base

C_{n_p} = Cn/(pd/V), pd/V = 0.5 at M = 0.91; pd/V = 0.2 at M = 3.02

C_Y = side force coefficient

C_{Y_p} = C_Y/(pd/V), pd/V = 0.5 at M = 0.91; pd/V = 0.2 at M = 3.02

d = model diameter at a cylinder cross section

p = model spin rate, radians/sec

pd/V = dimensionless spin rate

S = reference area, (3.1416)*d*d/4

V = free-stream velocity

X_{cp} = C_m/C_N, normal force center of pressure

Y_{cp} = C_n/C_Y, side (Magnus) force center of pressure

DISTRIBUTION LIST

No. of Copies	Organization
12	Administrator Defense Technical Info Center ATTN: DTIC-DDA Cameron Station Alexandria, VA 22304-6145
1	HQDA DAMA-ART-M Washington, DC 20310
1	Commander US Army Materiel Command ATTN: AMCDRA-ST 5001 Eisenhower Avenue Alexandria, VA 22333-0001
8	Commander Armament RD&E Center US Army AMCCOM ATTN: SMCAR-TDC SMCAR-TSS SMCAR-LCA-F Mr. D. Mertz Mr. E. Falkowski Mr. A. Loeb Mr. R. Kline Mr. S. Kahn Mr. H. Hudgins Dover, NJ 07801-5001
1	Commander US Army Armament, Munitions and Chemical Command ATTN: AMSMC-LEP-L Rock Island, IL 61299
1	Director Benet Weapons Laboratory Armament RD&E Center US Army AMCCOM ATTN: SMCAR-LCB-TL Watervliet, NY 12189
1	Commander US Army Armament, Munitions and Chemical Command ATTN: SMCAR-ESP-L Rock Island, IL 61299

No. of Copies	Organization
1	Commander US Army Aviation Research and Development Command ATTN: AMSAV-E 4300 Goodfellow Blvd St. Louis, MO 63120
1	Director US Army Air Mobility Research and Development Command Ames Research Center Moffett Field, CA 94035
1	Commander US Army Communications - Electronics Command ATTN: AMSEL-ED Fort Monmouth, NJ 07703
1	Commander ERADCOM Technical Library ATTN: DELSD-L (Reports Section) Fort Monmouth, NJ 07703-5301
3	Commander US Army Missile Command Research, Development & Engineering Center ATTN: AMSMI-RD Dr. Bill Walker Mr. R. Deep Redstone Arsenal, AL 35898
1	Director US Army Missile & Space Intelligence Center ATTN: AIAMS-YDL Redstone Arsenal, AL 35898-5000
1	Commander US Army Tank Automotive Command ATTN: AMSTA-TSL Warren, MI 48397-5000
1	Director US Army TRADOC Systems Analysis Activity ATTN: ATAA-SL White Sands Missile Range, NM 88002

DISTRIBUTION LIST

No. of Copies	Organization
1	Commander US Army Research Office P. O. Box 12211 Research Triangle Park, NC 27709
1	Commander US Naval Air Systems Command ATTN: AIR-604 Washington, DC 20360
2	Commander David W. Taylor Naval Ship Research and Development Center ATTN: Dr. S. de los Santos Mr. Stanley Gottlieb Bethesda, Maryland 20084
2	Commander US Naval Surface Weapons Center ATTN: Dr. T. Clare, Code DK20 Dr. F. Moore Dahlgren, VA 22448-5000
1	Commander US Naval Surface Weapons Center ATTN: Dr. U. Jettmar Silver Spring, MD 20902-5000
1	Commander US Naval Weapons Center ATTN: Code 3431, Tech Lib China Lake, CA 93555
1	Commander US Army Development and Employment Agency ATTN: MODE-TED-SAB Fort Lewis, WA 98433
1	Director NASA Langley Research Center ATTN: NS-185, Tech Lib Langley Station Hampton, VA 23365
2	Commandant US Army Infantry School ATTN: ATSH-CD-CSO-OR Fort Benning, GA 31905
1	Air Force Armament Laboratory ATTN: AFATL/DLODL Eglin AFB, FL 32542-5000
3	Sandia Laboratories ATTN: Technical Staff, Dr. W.L. Oberkampf Aeroballistics Division Dr. F. Blottner Albuquerque, NM 87184
3	Director NASA Ames Research Center ATTN: MS-227-8, L. Schiff MS-202A-14, D. Chaussee M. Rai Moffett Field, CA 94035
1	Massachusetts Institute of Technology ATTN: Tech Library 77 Massachusetts Avenue Cambridge, MA 02139
1	Virginia Polytechnic Institute & State University ATTN: Dr. Clark H. Lewis Department of Aerospace & Ocean Engineering Blacksburg, VA 24061
1	University of Delaware Mechanical and Aerospace Engineering Department ATTN: K. L. Palko Newark, DE 19711

DISTRIBUTION LIST

10 Central Intelligence Agency
Office of Central Reference
Dissemination Branch
Room GE-47 HQS
Washington, DC 20502

Aberdeen Proving Ground

Dir, USAMSAA
ATTN: AMXSY-D
AMXSY-MP, H. Cohen

Cdr, USATECOM
ATTN: AMSTE-TO-F

Cdr, CRDC, AMCCOM,
ATTN: SMCCR-RSP-A
SMCCR-MU
SMCCR-SPS-IL

USER EVALUATION SHEET/CHANGE OF ADDRESS

This Laboratory undertakes a continuing effort to improve the quality of the reports it publishes. Your comments/answers to the items/questions below will aid us in our efforts.

1. BRL Report Number_____ Date of Report_____

2. Date Report Received_____

3. Does this report satisfy a need? (Comment on purpose, related project, or other area of interest for which the report will be used.)_____

4. How specifically, is the report being used? (Information source, design data, procedure, source of ideas, etc.)_____

5. Has the information in this report led to any quantitative savings as far as man-hours or dollars saved, operating costs avoided or efficiencies achieved, etc? If so, please elaborate._____

6. General Comments. What do you think should be changed to improve future reports? (Indicate changes to organization, technical content, format, etc.)

CURRENT ADDRESS

Name

Organization

Address

City, State, Zip

7. If indicating a Change of Address or Address Correction, please provide the New or Correct Address in Block 6 above and the Old or Incorrect address below.

OLD ADDRESS

Name

Organization

Address

City, State, Zip

(Remove this sheet along the perforation, fold as indicated, staple or tape closed, and mail.)

END

10-86

DTIC